Use of a water mist for smoke confinement and radiation shielding in case of fire during tunnel construction

R. Mehaddi, Anthony Collin, Pascal Boulet, Z. Acem, J. Telassamou, S. Becker, F. Demeurie, Jean-Yves Morel

Version of Record: https://www.sciencedirect.com/science/article/pii/S1290072919301255
Manuscript_218b32b2fd36bc7e6af7aad70a0443e7

Proposition of communication in **International Journal of Thermal Sciences** [Version: September 20, 2019]

Use of a water mist for smoke confinement and radiation shielding in case of fire during tunnel construction

R. Mehaddi*(1), A. Collin(1), P. Boulet(1), Z. Acem(1), J. Telassamou(1), S. Becker(1), F. Demeurie(1) and J-Y. Morel(1)

(1) LEMTA, Université de Lorraine, CNRS

2 Avenue de la Forêt de Haye - TSA 60604 - 54518 Vandœuvre-lès-Nancy cedex, France

ABSTRACT

The ability of a water curtain to stop smoke and radiation from a fire is investigated in the particular configuration of a tunnel during construction work. Experiments are conducted in reduced scale ($1/22^{nd}$) in a blind tunnel and simulations are performed in small and real scale configurations. The small-scale experimental model consists of a 6.20 m long polycarbonate circular tunnel with a diameter of 40 cm. It is connected to a 1.20 m cubic space, which represents the wellbore of the tunnel boring machine. The scenario considers a fire occurring in the tunnel and the activation of a water mist downstream from the fire, close to the wellbore, in order to stop smoke and radiation emitted by the fire. The spraying system consists of 5 injection nozzles, regularly distributed on the ceiling of the tunnel. The numerical simulations are carried out using Fire Dynamics Simulator. The results from both small and large scale studies show that the water curtain induces a strong mixing of air and smoke due to drag effect, but it does not stop the smoke flow. Similarly, despite the down drag effect due to the curtain, fresh air continuously feeds the fire, crossing the mist area and flowing in the lowest part of the tunnel as a counter-current flow. Upstream from the water curtain the smoke

is filling all the tunnel due to a strong de-stratification, partially diluted with air in the lower counter-current flow. There may be a remaining thermal stratification, but contour plots of soot mass fraction show that soot particles are found even in the lowest part of the tunnel in a layer of smoke cooled by the spray and diluted with air. Radiation from the fire is attenuated as expected due to radiation and droplet interactions, with a radiation attenuation up to 90 $\%$ for the large scale water flow-rate investigated in the present case (15 m^3/h).

1. INTRODUCTION

In this article the use of a water curtain is studied in the case of a fire occurring in a tunnel during construction work. The practical underlying question is related to the conditions of escape for workers in the tunnel and to the possibility of action for firefighters. This problem was addressed in the frame of the french regulation, within a collaboration between the Société du Grand Paris company and the LEMTA laboratory. The water curtain is considered in the present work as a possible solution to improve the surrounding conditions in the tunnel or at least near the tunnel exit by creating a shield against smoke and heat. The scenario assumes that the last worker escaping from the near-fire area may activate a water spray system to protect the tunnel part downstream from this location. If such a shielding ability is proven, spray systems could be installed at given longitudinal positions in the tunnel to allow smoke and fire confinement. Consequently, the objectives are twofold: (i) to observe whether or not the water curtain may stop the smoke flow and allow a safe escape and access downstream from the water curtain, and (ii) to evaluate the radiation attenuation achieved with this water curtain. The originality of the problem is that the tunnel is under construction, which means that no ventilation device is operating to manage the smoke flow. This is why an alternate solution is sought to control the smoke flow. Secondly, only one end of the tunnel is open, the other one still being in the excavation phase (blind tunnel). Consequently, one can expect to observe differences when comparing the present situation with usual tunnel studies. Indeed, studies found in the literature usually and logically considered cases where the tunnel was open on both sides or where the spraying system was combined with longitudinal ventilation such as in Sun *et al.* (2016); Blanchard *et al.*

(2014); Ingason *et al.* (2016); Liang *et al.* (2017); Li *et al.* (2017), to name a few. Blanchard *et al.* (2014) focused on fires in an intermediate-scale tunnel (with a diameter of $2\,m$ and a length of $17.5\,m$) performing experiments and numerical simulations. By spraying directly on the fire, they showed that a significant part of the heat released by the fire was absorbed by the water drops and they focused on spray efficiency concerning the fire control. A longitudinal ventilation was also involved in this study. Some attention was paid to the smoke flow, but no observation of a possibility to stop the smoke was done in this study and water flow-rates were too low to allow such a possibility. Liang *et al.* (2017) studied numerically the interaction between a transverse ventilation and a water mist curtain in a large scale tunnel opened at both ends, in order to confine the fire zone in a limited area. Sun *et al.* (2016) performed a systematic experimental study on the interaction between a hot smoke layer and a water mist curtain with and without longitudinal ventilation. Based on temperature observations, they showed that the water mist stops the smoke layer and that the efficiency of this confinement is reduced by the longitudinal ventilation. The tunnel was also opened at both ends allowing the system to keep a near-constant pressure. Moreover, in their study, Sun *et al.* (2016) used five rows of water curtains while in the present study only one row is considered. Furthermore, The interaction of the smoke layer with a sprinkler or a water mist was studied by several authors such as Bullen (1983), Tang *et al.* (2013) and Wang *et al.* (2018) to name a few. Bullen (1983) and Tang *et al.* (2013) considered the interaction of a sprinkler with a stagnant layer of smoke. In that case, Tang *et al.* (2014) devlopped a theoretical model based on that of Bullen (1983). In their study, they show that in the case of high sprinkler flow rates, the smoke can be strongly pushed downward by the spray which leads to a strong mixing between the ambient air and the smoke layer. In the specific case of long channel (tunnel, corridor) where the smoke flow has a horizontal velocity, Wang *et al.* (2018) observed that the smoke falls on the floor due to the water mist. Moover, these authors observed a lowering of the smoke layer downwstream of the water mist. In addition, upstream of the spray, they observed, an improvement in visibility conditions and a decrease in CO concentration. Recently Yang *et al.* (2019) studied numerically the smoke control with water mist in a tunnel in construction. They showed that even if the CO concentration was decreased, the soot density was largely increased and the visibility

was also decreased at the lower part of the water tunnel.

In the present study, we are concerned with a tunnel in the construction phase, with no longitudinal ventilation possibly penalizing the down drag of the smoke by the spray. However, one tunnel's end is closed, which will affect the smoke extraction and induce a significant pressure increase. In this case, it is relevant to ask whether or not the smoke layer can still be confined by the spraying system.

Radiative transfer from fire and corresponding attenuation by a water spray is another issue, which can be almost addressed uncombined from the rest of the problem. The use of water sprays as radiative shields has received a lot of attention in the past decades. It is now well known that droplets absorb and scatter radiation emitted from the fire, with an efficiency governed by droplet size, water concentration and water curtain thickness (Dembélé *et al.*, 2001; Collin *et al.*, 2007, 2010, to name but a few). By using the right water injection conditions, there is no doubt that high attenuation efficiency can be reached. Knowing these injection characteristics from measurements or simulation allows predicting the radiation attenuation using numerical simulations as in Collin *et al.* (2007) for example.

Tests devoted to these problems of smoke/spray interactions and radiation attenuation can be hardly conducted at real scale, but reduced scale experiments can be used if scaling rules are fulfilled. Then, numerical simulations can be conducted at reduced scale to validate the numerical approach and to provide additional results which could not be directly measured such as the velocity and soot concentration fields. The paper by Ingason & Li (2010) for example provides scaling factors for the main parameters involved in the problem, i.e. geometry, HRR, water flow-rate and droplet size. Relevant experiments can be analyzed, with observations possibly extended to the real scale. Finally, full scale simulations can provide supplementary answers to the present questions of smoke control and radiation attenuation at real scale. Small scale experiments and numerical simulations were combined in the present work, using Fire Dynamics Simulator (FDS v.6) for smoke flow simulations and home-made computations for radiative transfer evaluation. The interaction mechanisms were observed, in particular cooling, drag and de-stratification effects.

The experimental setup and the numerical simulations are presented in the following sections, emphasizing the original context of a tunnel in its construction phase. Results are discussed,

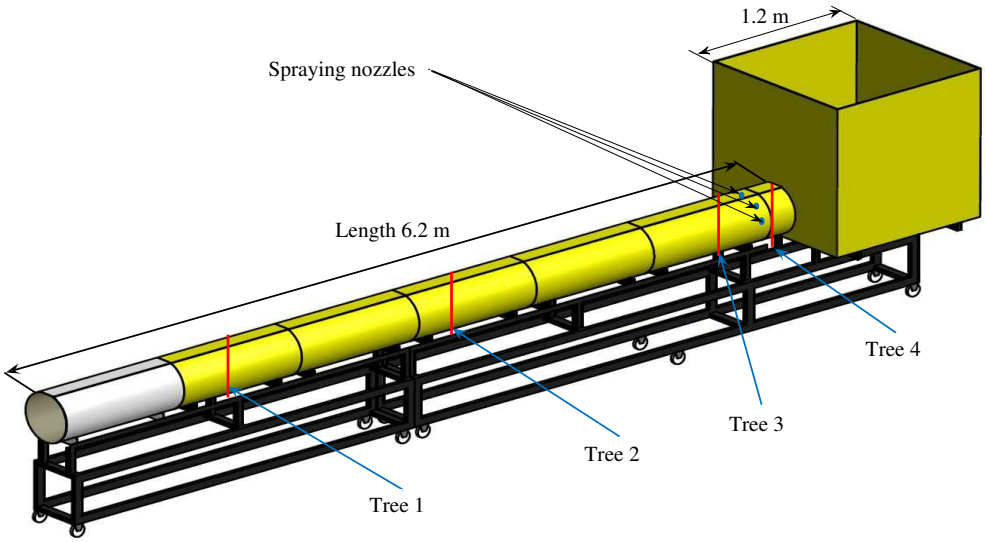

Figure 1: Schematic view of the experimental setup at small scale.

particularly focusing on the smoke flow alteration. A sensitivity study is also presented, varying the configuration and the water spray characteristics to provide a more detailed answer on the capability of the water curtain to stop the smoke flow. Then, the problem of radiation attenuation is addressed in a separate section.

2. EXPERIMENTAL STUDY

2.1 Experimental setup

The experimental setup is schematically shown in Figure 1. A 6.20 m long tunnel with a diameter of 40 cm is connected to a 1.20 m cube, which mimics a station or a wellbore for the tunnel boring machine. The fire is produced at the blind side of the tunnel in a section made of steel in order to withstand the high temperatures. Pool fires burning heptane are used to reproduce the fire. The rest of the setup is made of transparent polycarbonate sections to allow an easy visualization of the smoke flow. The spraying system of the lab-scale tunnel is presented in Figure 2. Five nozzles are connected in series

on a feeding pipe, below the tunnel ceiling, with a $45°$ spacing angle between two successive nozzles. Nozzles referred to as TP400067 by Spraying systems and Co were used. Two water pressures were studied ($4\ bars$ and $1.5\ bars$). Results are only commented here for the pressure set to $4\ bars$. The corresponding water flow-rate is $0.32\ L/min$. The droplet distribution was measured by Lechêne *et al.* (2011) using a Phase Doppler Particle Analyser (PDPA). They found that the best description of the droplets distribution was a log-normal law with mean diameter set to $123\ \mu m$ with a dispersion parameter equal to 0.4. The feeding pressure of the nozzles, was controlled with a pressure sensor (see Figure 2). Note that the mean diameter is not an arithmetic mean of the droplets diameter. It is a parameter that allows to define the best fit of the experimental data.

The dimensions and parameters at the full scale were defined with the *Société du Grand Paris* company. Actually, the present problem of water curtain efficiency was raised for a tunnel diameter of 8.70 m and a wellbore 30 m deep. This geometrical configuration and the corresponding water curtain injection with five sprays were taken from a real situation used in one recent construction site for the underground extension in Paris. The maximum HRR was set to 10 MW to allow a significant heat load, still being realistic considering the particular situation of tunnel construction. Preliminary simulations showed that a higher HRR in the present configuration could be hardly achieved since no ventilation device is involved, or if already designed the ventilation system is supposed to be turned off or damaged due to the fire. This means that air can be only naturally supplied to the fire. Tests with higher HRR resulted in under-ventilated conditions and even numerical instabilities, as such a HRR was not allowed by the available oxygen near the fire area. 10 MW was found as a quite large HRR, for which air supply is still large enough to keep the fire burning. Regarding the water flow-rate, a maximum value of 15m^3/h was set considering the available water volume in the construction conditions.

A comparison of the conditions at both scales can be done based on scaling rules. the starting point is the diameter set to 40 cm for the model, corresponding to 8.70 m at real scale. Table 1 presents a summary of the main parameters. The prescribed real scale conditions are given on the second line with the corresponding conditions that should be involved at reduced scale to achieve complete

Table 1: Scaling conditions

	parameter	**scaling factor**	**Studied conditions** [Corresponding parameters after scaling are in brackets]
Real scale tunnel			Large scale [corresponding small scale]
	tunnel length	L	500 m [22.70 m]
	tunnel diameter	L	8.70 m [0.40 m]
	wellbore size	L	30 m [1.36 m]
	HRR	$L^{5/2}$	10 MW [4.4 kW]
	water flow-rate	$L^{5/2}$	15 m^3/h [6.6 L/h]
	droplet size	$L^{1/2}$	500 μm [107 μm]
Small scale experiments			Small scale [corresponding large scale]
	tunnel length	L	6.20 m [136 m]
	tunnel diameter	L	0.40 m [8.70 m]
	wellbore size	L	1.20 m [26 m]
	HRR	$L^{5/2}$	3.5 kW [8.7 MW]
	water flow-rate	$L^{5/2}$	122 L/h [286 m^3/h]
	droplet size	$L^{1/2}$	123 μm (580 μm]

scaling conditions (in brackets).

The reduced scale conditions cannot be fulfilled exactly. For example, a 22.70 m long tunnel cannot be used and the available nozzles cannot produce the water injection characteristics which are prescribed by the scaling rules. Instead, reasonable experimental conditions are used in the reduced scale study, as presented in the third line, with their corresponding conditions which would occur at full scale (in brackets). As can be seen, some conditions are well fulfilled concerning the geometry (close values for the wellbore and the tunnel diameter) and the fire HRR. However, the water flow-rate and the droplet size are different. This is why the numerical simulations were also used to complete the study.

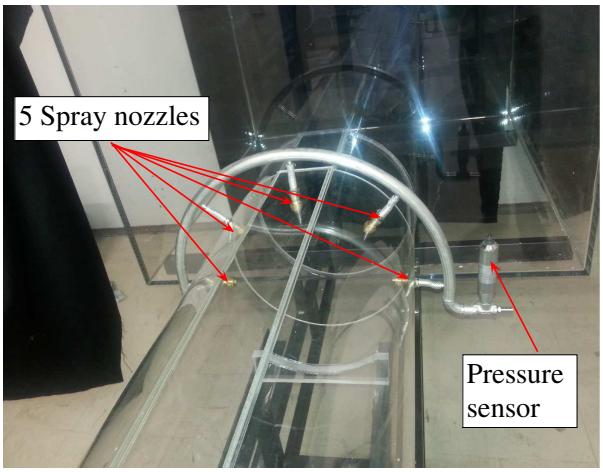

Figure 2: Spraying system configuration.

Simulations with FDS were first used for a validation purpose based on comparisons with the small scale experiments. Then, in a second step, simulations were conducted with the real scale conditions. Considering the gap in the water flow-rates in particular, some differences are expected between the different cases. Then, simulations performed in various conditions can be carried out at both scales to fulfil all the scaling conditions, in order to check that the same results are obtained and to perform a sensitivity study.

To measure the temperature distribution, 76 K-type thermocouples were used, distributed over 4 vertical thermocouple trees (19 thermocouples for each thermocouples tree) spaced by $2\ cm$. These thermocouple trees, referred to as tree 1 to tree 4 in Figure 1, are respectively located at 4.26 m (tree 1), 2.26 m (tree 2), 0.62 m (tree 3) and 0.045 m (tree 4) from the tunnel exit toward the wellbore side. They provide the vertical temperature profiles in the vicinity of the fire zone (tree 1), in the middle of the tunnel (tree 2) and upstream of and downstream from the water curtain area (tree 3 and tree 4).

The fire was generated by heptane pools with diameters $68\,mm$ and $81\,mm$. They were designed with a $4\ cm$ depth, made of steel with $4\ mm$ thick walls. The initial fuel quantity was $30\ g$ corresponding to $1\ cm$ height of Heptane. A high precision balance was used to measure the fuel mass loss, from

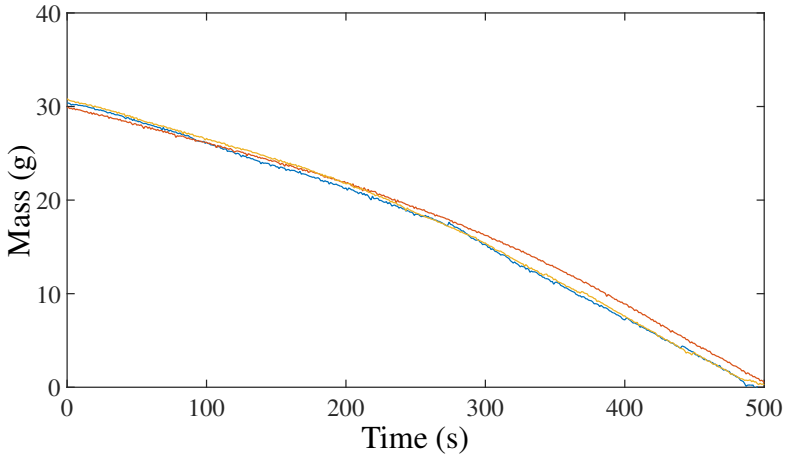

(a)

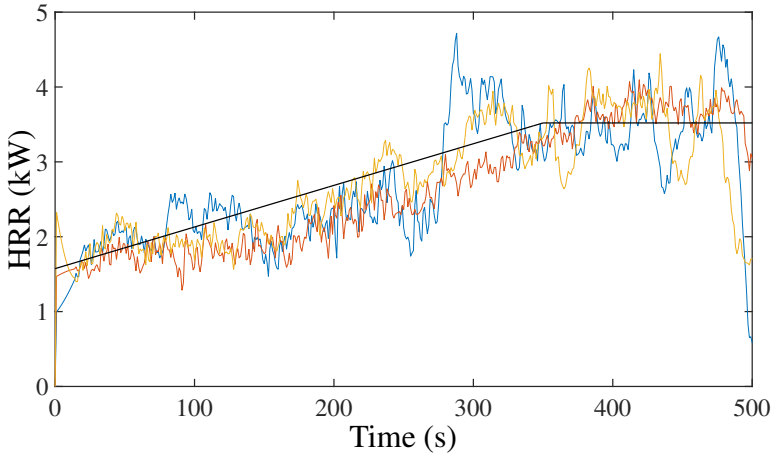

(b)

Figure 3: Time evolution of mass (a) and heat release rate (b) for a heptane pool diameter $81\,mm$. The coloured continuous lines corresponds to the experimental data and the solid black line corresponds to the best fit used for the numerical simulation in FDS.

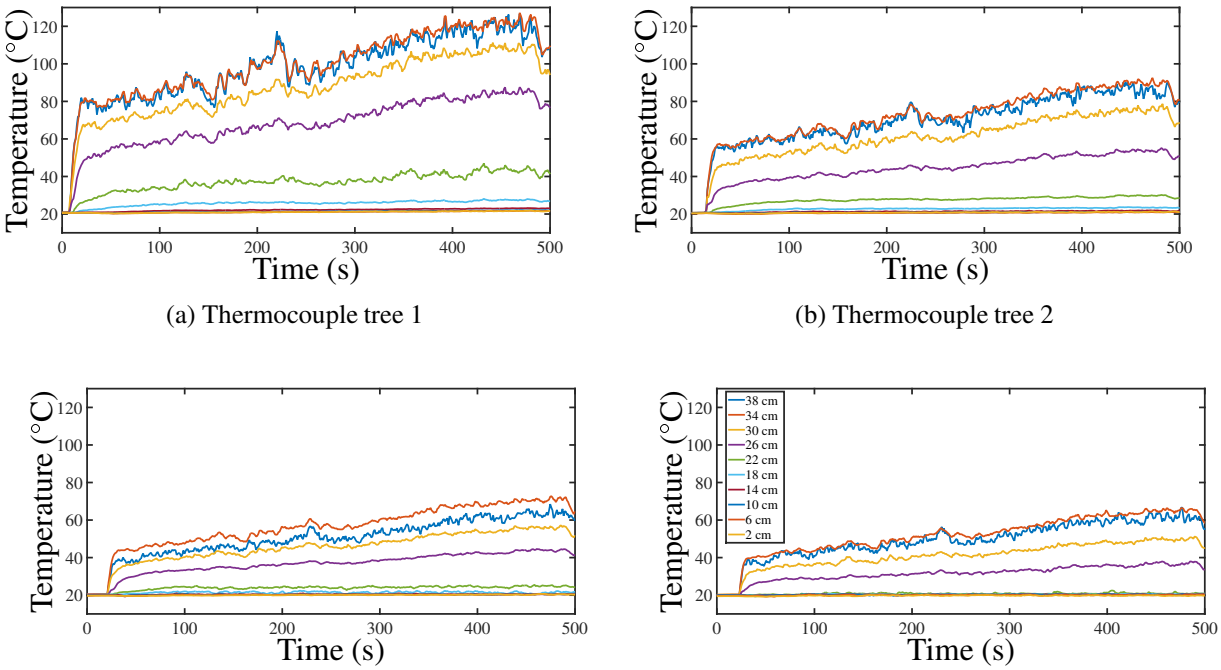

(a) Thermocouple tree 1

(b) Thermocouple tree 2

(c) Thermocouple tree 3

(d) Thermocouple tree 4

Figure 4: Time evolution of the temperature for all thermocouple trees without spray. The pool diameter is 81 mm and the HRR is 3.5 kW. Correspondence between lines and thermocouple positions is indicated in the bottom right subfigure.

which the heat release rate was calculated. The tests were defined with the following steps: initial fuel weighing, pool fire ignition with a spark igniter to avoid any disturbance of the fire zone during this initial step, activation of the spraying system after $300\,s$, and continuous spray discharge during $200\,s$. An experiment was also conducted without spray activation to allow comparisons and evaluation of the spray influence. The reproducibility of the experiments was checked by performing three identical tests for each of the investigated cases.

The heat release rate was estimated, simply involving the mass loss rate dm/dt and the heat of combustion Δh_c for heptane with the following relationship

$$Q = -\Delta h_c \frac{dm}{dt}\,, \tag{1}$$

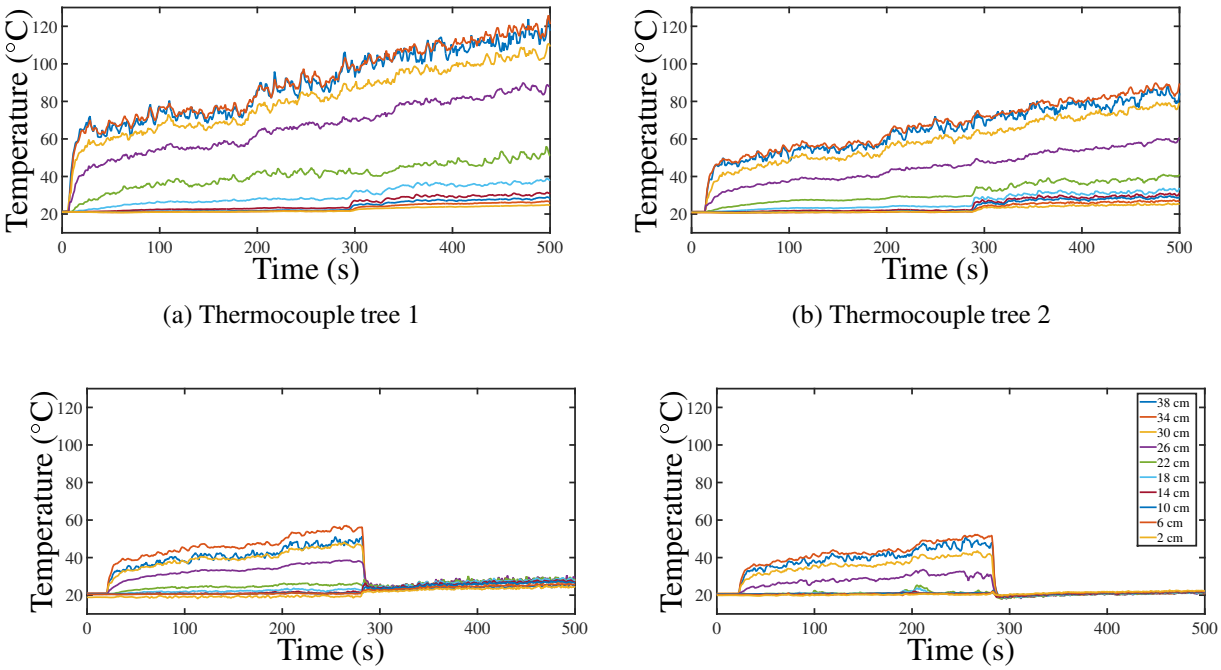

(a) Thermocouple tree 1

(b) Thermocouple tree 2

(c) Thermocouple tree 3

(d) Thermocouple tree 4

Figure 5: Time evolution of the temperature for all thermocouple trees with spray activation after 300 s. The HRR is 3.5 kW and the water pressure feed is 4 bars.

with $\Delta h_c = 44.6\ kJ/g$ based on Babrauskas (1983). Note that this formulation assumes complete combustion. Of course this is questionable, but no attempt was conducted here to tune this HRR as the combustion yield would be ascertained. It was decided to compare the results keeping in mind this possible inaccuracy source and focusing on the effects related to the aspersion activation.

As an example, the mass loss rate for the 81 mm pool and the corresponding (HRR) are presented in Figures 3a and 3b. The HRR increases in a first step because of progressive heating of the steel structure of the tunnel in this area, which results in a heat feedback from the walls. This phase was approximated as a linear increase of the HRR during the first 350 s in our simulations. Then, a plateau is reached around 3.5 kW, which corresponds to a full-scale HRR equal to 8.7 MW, as seen in Table 1. Note that this behaviour is different from the findings by Hayasaka (1997) who observed two steady values of the HRR during the fire burning. This difference can be explained by the fact that Hayasaka

(1997) considered pool fires in an open environment. However, for the 68 mm pool fire (not shown here), two steady values of the HRR are observed due to the fact that the pool fire is small such that the fire behaves as in an unbounded environment. In this case the maximum HRR was 2.2 kW.

2.2 Experimental results

Temperature measurements are gathered on Figures 4 and 5 for the cases without and with spray activation, respectively. Rough data are provided as a function of time, each sub-figure corresponding to a given thermocouple tree. Only the case of the 81 mm diameter pool is presented, as the same observations hold for the 68 mm case (with a lower temperature increase). As expected, a progressive increase with time is observed for the temperature, as the walls are progressively heated by the smoke flow. The stratification is obvious, with an upper hot smoke layer surrounding a fresh smoke-free layer, as confirmed by direct observations. When the spray is activated after 300 s (Figure 5) temperatures close to the spray area are strongly affected, all curves collapsing according to data given by the trees 3 and 4. This is a consequence of strong drag and cooling effects resulting in a thermal de-stratification. Tree 1 (close to the fire) and tree 2 (in the middle of the tunnel) are less affected, but the effect of the spray activation is still visible, with a small overshoot slightly delayed, since the perturbation reaches these positions later. Thermal stratification obviously persists in this area, while direct observation shows that smoke is dragged in the lower part upstream from the water curtain. This dragged smoke is probably cooled down in the spray area and surrounded by hot smoke directly produced by the fire, explaining why thermal stratification is still observed.

By using the temperature measurements provided by the thermocouple trees in the tunnel, the height of the smoke layer can be estimated. Indeed, the method of Janssens and Tran (1992) allows calculating this height by using the vertical temperature profiles. By supposing that the lower layer of fresh air has a constant temperature, the thickness of the upper layer (smoke layer thickness $H - Z_{int}$) is calculated by solving the following set of equations

$$(H - Z_{int})T_{up} + Z_{int}\,T_{low} = \int_0^H T(z)\,dz\,, \tag{2}$$

$$(H - Z_{int})\frac{1}{T_{up}} + \frac{Z_{int}}{T_{up}} = \int_0^H \frac{1}{T(z)}\,dz\,, \tag{3}$$

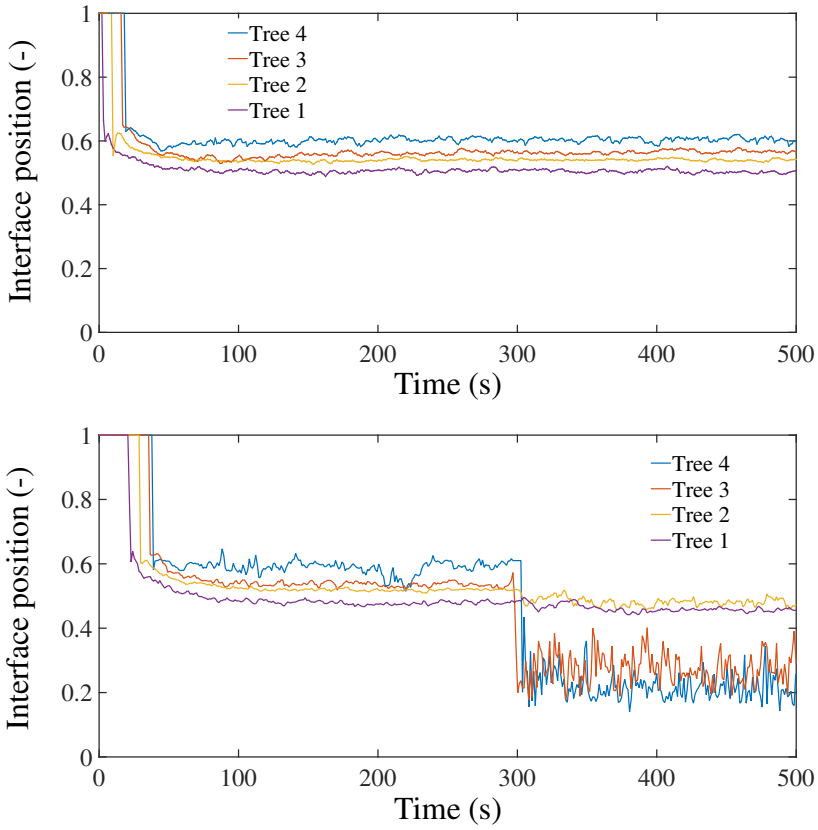

Figure 6: Time evolution of the position of the interface between air and smoke layer, without spray (upper subfigure) and with spray activation after 300 s (bottom). Case of a pool fire of diameter 81 mm.

where T_{up} is the upper layer temperature (temperature of the smoke layer), T_{low} is the lower layer one, which is assumed to be equal to the air temperature at the ground (i.e. $T_{low} = T(0)$), Z_{int} is the position of the interface between the smoke layer and the fresh air (non-dimensionalized dividing by the tunnel diameter), H corresponds to the tunnel diameter and z is the vertical coordinate. Note that this method have been compared by Haouari-Harrak *et al.* (2019) to several methods such as least-squares and integral ratio by He *et al.* (1998), N-percent method developed by Cooper *et al.* (1982) and image processing method. The conclusion of this comparison is that the method of Janssens and Tran provides results very close to the ones obtained with the image processing method. This is the reason why we choose this method for the present study.

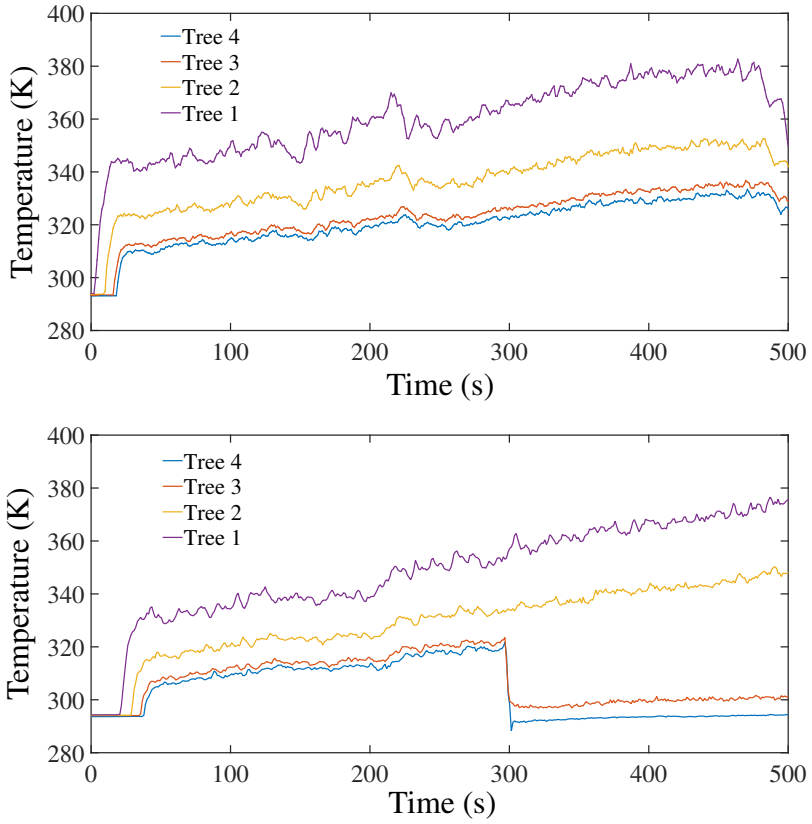

Figure 7: Time evolution of the average temperature of the smoke layer, without spray (upper subfigure) and with spray activation after 300 s (bottom). Case of a pool fire of diameter $81\ mm$.

Figure 6 shows the variation of the smoke layer interface position Z_{int} as a function of time, with and without spray activation, for a pool diameter $D_c = 81\ mm$ and at the locations of the four thermocouple trees. It can be observed that, in both cases, the smoke layer thickness reaches rapidly a steady value. This value lies approximatively between 50% and 60% of the tunnel height, with a smoke layer thickness slightly decreasing with the longitudinal position.

When the spray is activated (after 300 s on the bottom subfigure), a sudden mixing occurs near the spray (Trees 3 and 4), while the smoke layer is weakly affected upstream from the spray, at least according to the present analysis of the temperature profiles. Note that the method still provides a remaining smoke-free layer near the spray, with a thickness around 20% of the tunnel height, which is a consequence of an analysis only based on the temperature in a situation of near flat temperature

profile which does not lead to an accurate application of the method. The visual observation rather indicates a mixing on the whole section.

Relations (2) and (3) also allows the mean temperature of the upper layer T_{up} to be calculated. The results are shown in Figure 7 for the same pool diameter $D_c = 81\ mm$. The average temperature of the smoke layer is constantly increasing with time, while the smoke layer has a constant thickness, as above-discussed.

When the spray is activated, the temperature close to the spray falls to the ambient one, almost instantaneously (as observed in Figure 5). This could be interpreted as an indication that smoke is blocked and does not cross the spray, but again this in contradiction with the visual observation. The mixing is obvious, but the method only based on the temperature profile analysis is no more suitable for an observation of the smoke in the present case, because the profile is no more contrasted between a hot smoke layer and a cold smoke-free layer. Note also that water affects the temperature measurement as thermocouples are not protected against direct impact and cooling (these thermocouples were rather designed to characterize the smoke flow before spray activation, after spray activation they were only used for a qualitative analysis). Again, the temperature criterion indicates that there is no stratification at all in the sprinkling zone and the low temperatures could lead to a conclusion that smoke do not cross the water curtain. However, visual observation indicates some smoke still escaping in the wellbore. This will be further commented below, using data which were obtained numerically for the soot concentration.

3. NUMERICAL SIMULATION

Numerical simulations have been conducted using the Fire Dynamics Simulator (FDS version 6.0.2), the CFD code developed by the National Institute of Standards and Technology (NIST), dedicated to the 3D simulation of fire related phenomena (McGrattan *et al.* , 2013).

Main dimensions and conditions are given in Table 2, with supplementary numerical parameters involved in the simulation. The thermal properties of the materials used for the simulations are also listed in table 3. The reduced- scale case involves 2.7 millions of cells and the large scale 9.4 millions.

Table 2: Numerical parameters used in the FDS simulations

Case study	**parameters**	**values**
Reduced scale	Tunnel size	length 6 m, diameter 0.40 m
	Grid size	1 cm cubic cells
	boundary conditions	1 cm thick steel or polycarbonate
	HRR	3.5 kW
	water flow-rate	122-6 L/h
	droplet size	123 μm (polydispersion described as a log normal law)
Real scale	Tunnel size	length 500 m, diameter 8.70 m
	Grid size	20 cm cubic cells
	boundary conditions	200 m ground thick
	HRR	10MW
	water flow-rate	15 m^3/h
	droplet size	100, 500 or 1000μm (monodispersed)

Table 3: Material properties used for simulations

Material –	**density** (kg/m^3)	**conductivity** $(W/(m\ K))$	**Emissivity** –	**Specific heat** $(J/(kgK))$
Polycarbonate	1200	0.2	0.9	1400
Steel	7850	45.8	0.95	460
Concrete (ground)	2100	1.6	0.9	1000

Prescribed HRR are used up to the stationary values indicated in Table 2, with a linear ramp from 0 up to a plateau at 3.5 kW after 350 s for the reduced scale (based on experimental observations) and to 10 MW after 200 s for the large scale (in agreement with the defined scenario). For the simulations

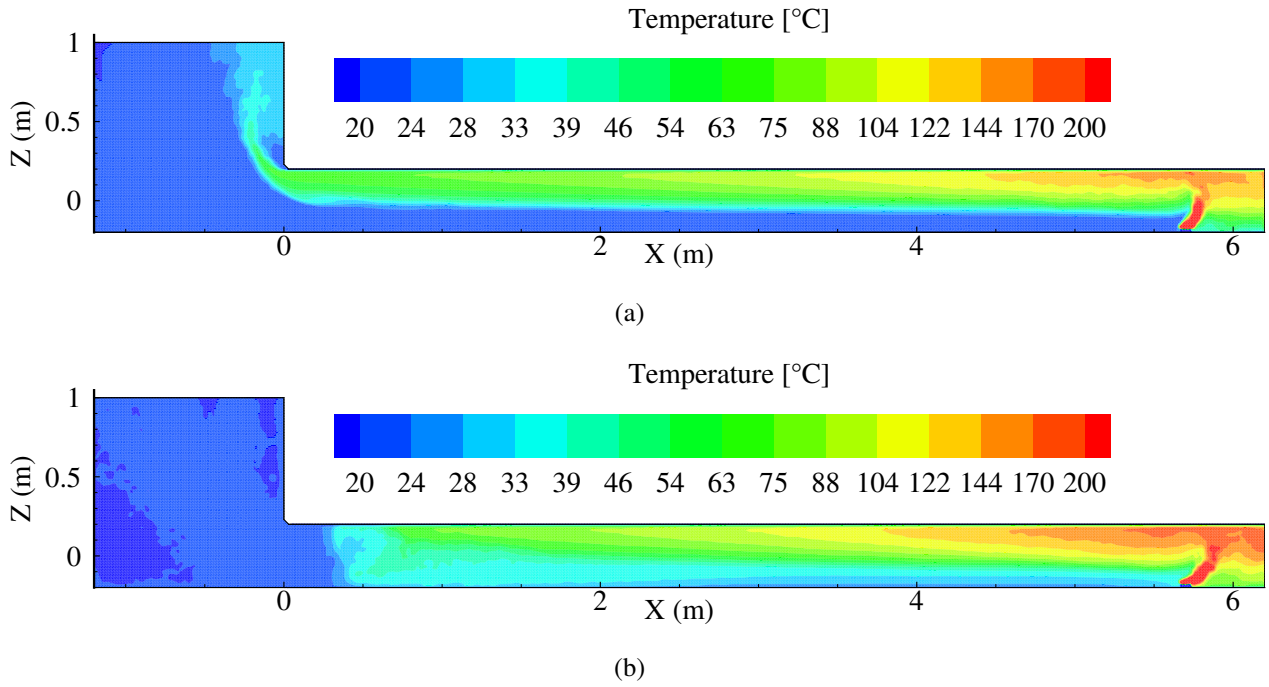

Figure 8: Contour plots of the temperature distribution in the case of HRR of 3.5 kW and the water flow-rate of 122 L/h. (a) corresponds to $t = 280s$ (20 s before spray activation), (b) corresponds to $t = 380$ s (80 s after spray activation). The slice plane passes centrally through the tunnel.

of the water mist, in the small scale simulations, the spray has elliptical cross section with angles of $20°$ and $8°$ at $1.5\,bars$ while at $4\,bars$ the angles were $48°$ and $18.5°$. For both cases, the droplets size distribution was a lognormal law. In the large scale simulations, the spray was conical with circular cross section with an angle of $60°$. The droplets sizes distribution was uniform in the large scale.

3.1 Small-scale configuration

Results are first commented in terms of temperature distributions. Figure 8 shows contour plots of temperature distribution 20 s before spray activation and 80 s after spray activation in the case of the HRR of 3.5 kW and for a water flow-rate of 122 L/h. Note that, only the case of the HRR of 3.5 kW will be presented through this section (comments would be similar for the 2.2 kW HRR case). A good description of the smoke stratification is observed before spray activation. In addition, the thickness

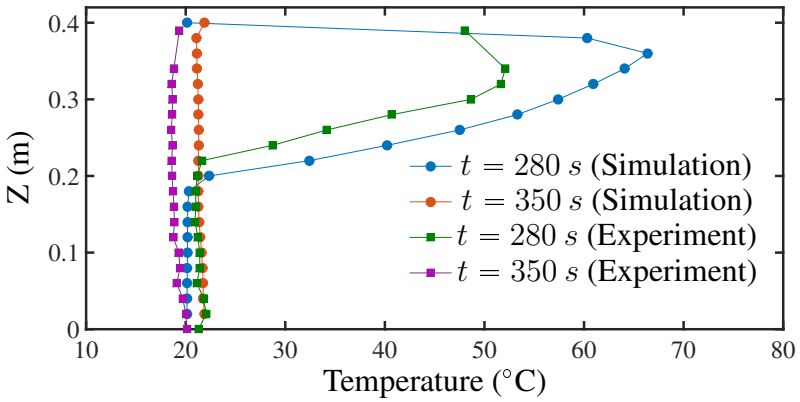

Figure 9: Temperature profiles obtained numerically and experimentally at position $x = 0.045\,m$ and at two instants $t = 280\ s$ and $t = 350\ s$.

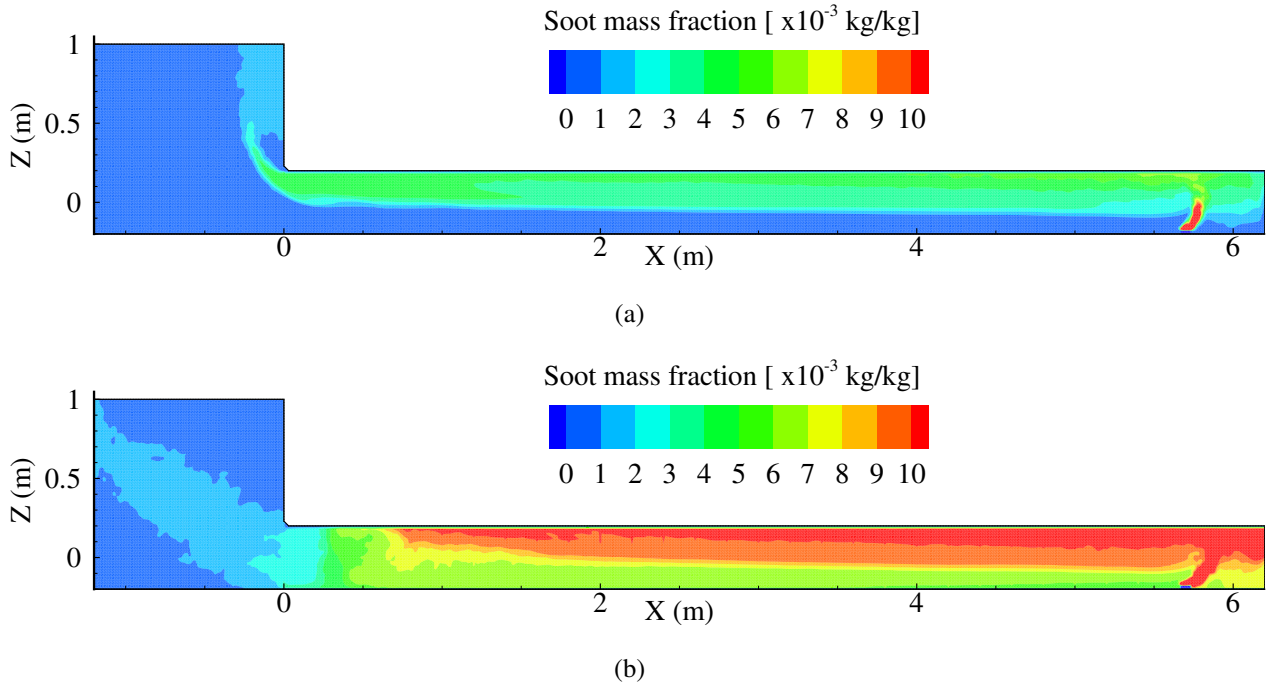

Figure 10: Contour plots of the soot mass fraction at $t = 380\ s$ after the beginning of the simulation in the case of HRR of 3.5 kW and the water flow-rate of 122 L/h. (a) corresponds to $t = 280s$ (20 s before spray activation), (b) corresponds to $t = 380\ s$ (80 s after spray activation).

of the smoke layer is in agreement with the experimental evaluation at $40\% - 50\%$ of the tunnel diameter (see Figure 8a). After activating the sprinklers, Figure 8b shows a thermal de-stratification of the smoke in the sprinkling zone. Moreover, a complete cooling of the smoke flow is observed in the wellbore while a thermal stratification is kept in the rest of the tunnel, in agreement with the experimental observation.

To complete this observation, the temperature profile simulated at the tree 4 position is shown in Figure 9, before spray activation (280 s) and during aspersion (350 s). Before aspersion, the smoke layer is clearly evidenced by a hot upper layer surrounding a layer at ambient temperature. Note that the comparison between experimental and numerical data is quite satisfactory regarding the temperature value (whereas no tuning was sought, by introducing an estimated combustion yield for example). In particular the position of the interface at around midheight of the tunnel is very well captured. During aspersion, experimental data indicates a strong cooling with a flat temperature profile at ambient value, which is also predicted by the simulation. It confirms that the flow is completely cooled at the exit of the tunnel, as seen in Figure 5d. Note that in appendix II, more comparisons are provided which confirm the ability of FDS6 software to well reproduce the experimental data.

In order to decide whether the smoke is blocked by the sprinkler system, contour plots of soot mass fraction are shown in Figure 10 at the same moments chosen for the temperature contours. It is seen in Figure 10b that the flow is mixed in the region of the sprinkler system but without preventing the smoke escape toward the wellbore side. This confirms the experimental observations. In order to understand this observation a zoom in the sprinklers zone and the wellbore is plotted in Figure 11. It is seen that the jet produced by the sprinklers drags the smoke flow coming from the fire side and the fresh air coming from outside. This mixture is then projected to the ground and produces a jet of cooled smoke which flows toward both sides. This is clearly demonstrated by the streamlines in Figure 11.

The software FDS6 calculates the energy conducted through walls (noted Q_{cond}). This quantity is divided by the fire heat release rate and plotted in figure (12). It can be seen that the conduction through walls is an important fraction of heat losses. The conduction part is of the order of 45 $\%$ of

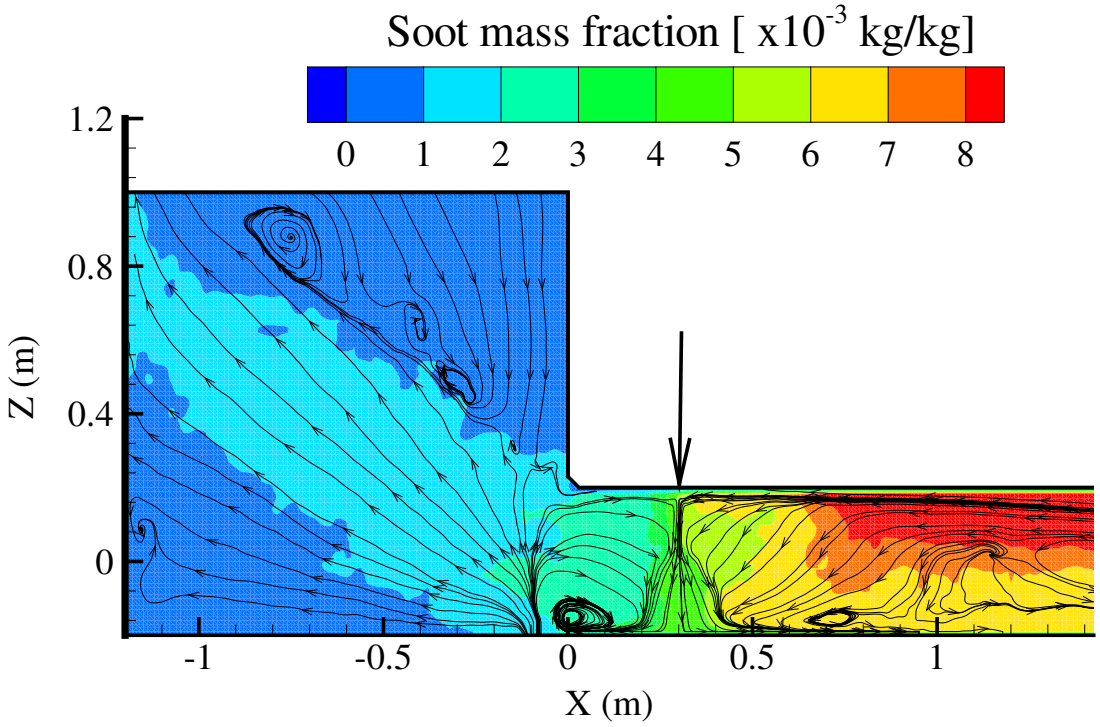

Figure 11: Contour plot of soot mass fraction with streamlines in the case of a HRR equal to 3.5 kW and a water flow-rate of 122 L/h. The arrow shows the position of the spray injection.

the fire heat release rate and increases to more than 53 % after the water mist was activated. This increase can be explained by the accumulation of smoke inside the tunnel.

In order to investigate the interaction between the smoke flow and the sprinkler system accurately, additional simulations have been carried out where the water flowrate of the spray has been varied. The considered flowrates are as follows: 6 L/h, 19 L/h and 75 L/h. Note that the 6 L/h case, corresponds to 15 m^3/h at the full scale (which was one of the prescriptions of the Société du Grand Paris company). This sensitivity study is conducted to investigate a wide range of water flowrates and to check that our conclusions on the inability to block the smoke is not conditionned by the particular flowrate set

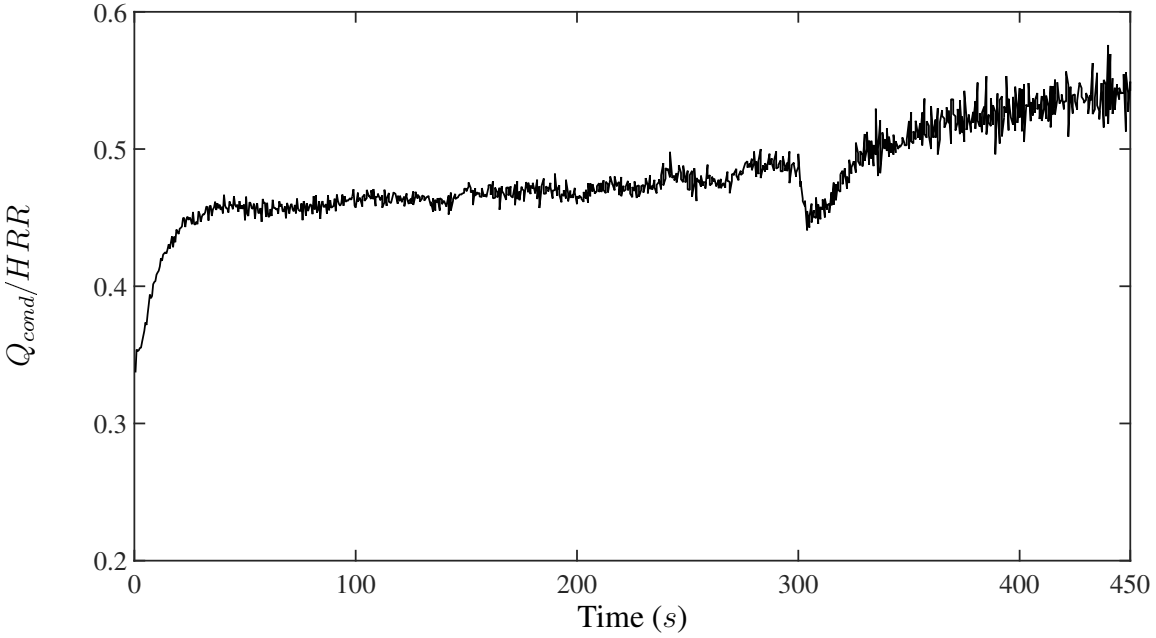

Figure 12: Variation of the ratio between the heat flux conducted through walls Q_{cond} and the fire heat release rate HRR, for three different droplets diameter .

in the previous paragraph.

For all these cases, contour plots of soot mass fraction are presented in Figure 13 at 380 s and 450 s after the fire ignition (the spray being activated after 300 seconds). It is seen that for small flowrates (see Figures 13a, 13b), the water, injected perpendicularly to the smoke flow, produces a mixing of smoke with fresh air in the sprinkling zone, without, however, preventing the smoke to flow towards the exterior of the computational domain. It is also seen that a counter-current is established in the lower part of tunnel, in the direction of the fire. This flow gradually fills the rest of the tunnel as shown in Figures 13a, 13b,13c and 13d. In the case of large water flow-rates, the momentum flux of the spray is so important that it develops as a free jet. However, owing to the entrainment induced by the jet, the smoke is not blocked by the water mist curtain. It is also interesting to note that, for median water flow-rates, a transitory behaviour occurs. It consists of a flapping behaviour of the spray which is either completely advected upstream or downstream of the tunnel. This is illustrated by Figure 14.

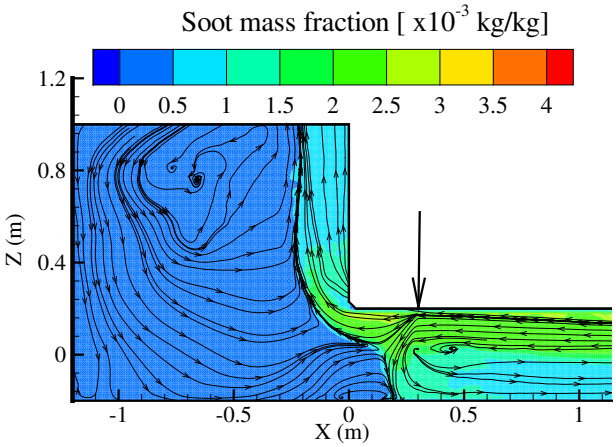

(a) Flow-rate of 6 L/h and $t = 380\ s$

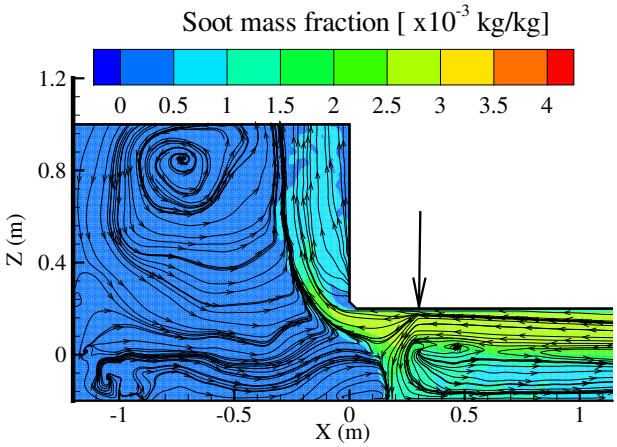

(b) Flow-rate of 6 L/h and $t = 450\ s$

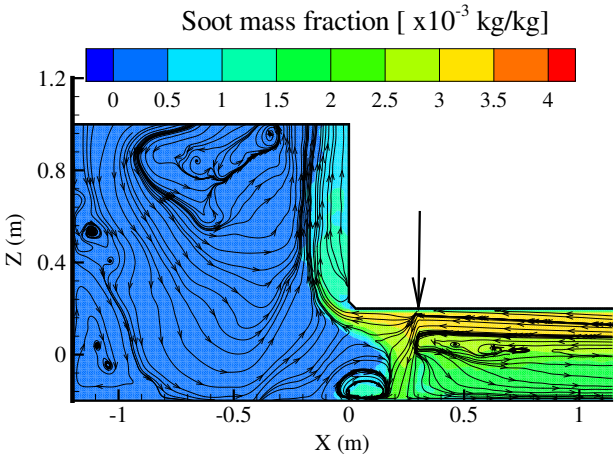

(c) Flow-rate of 19 L/h and $t = 380\ s$

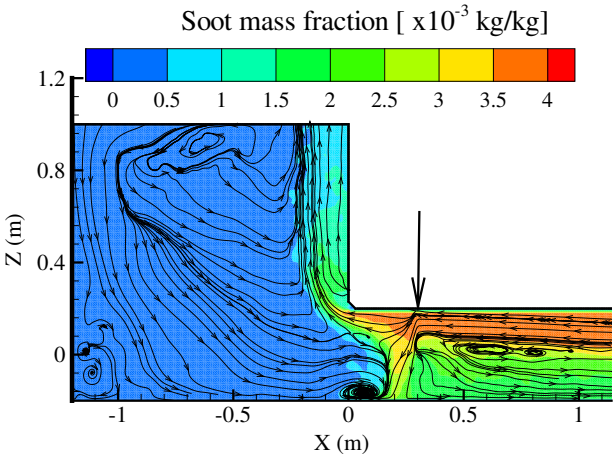

(d) Flow-rate of 19 L/h and $t = 450\ s$

Figure 13: continued in next page

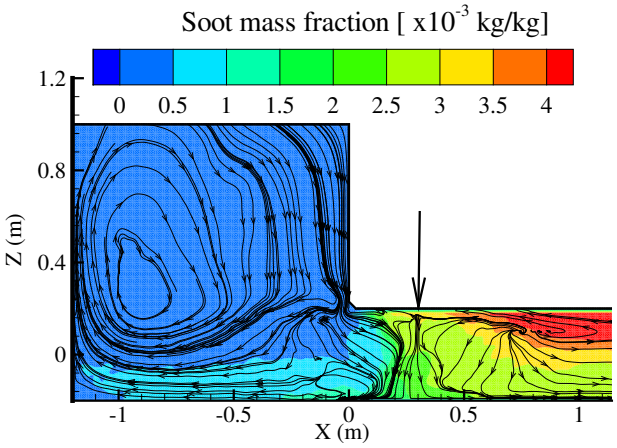

(e) Flow-rate of 75 L/h and $t = 380\ s$

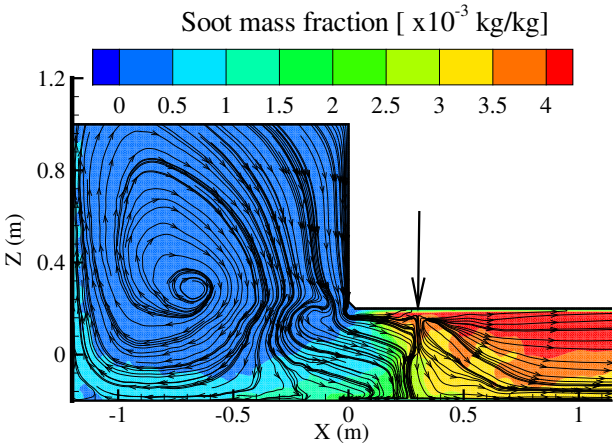

(f) Flow-rate of 75 L/h and $t = 450\ s$

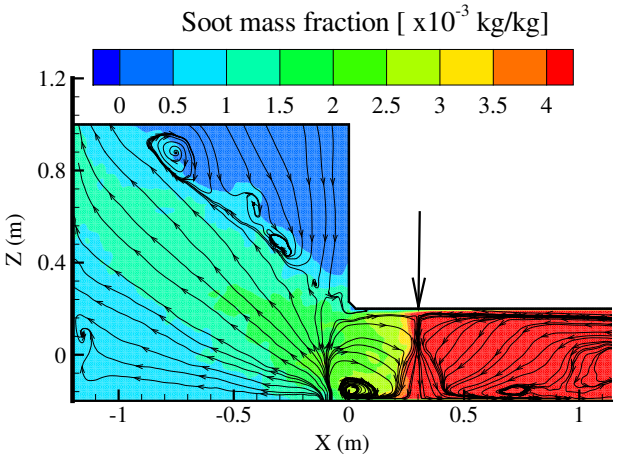

(g) Flow-rate of 122 l/h and $t = 380\ s$

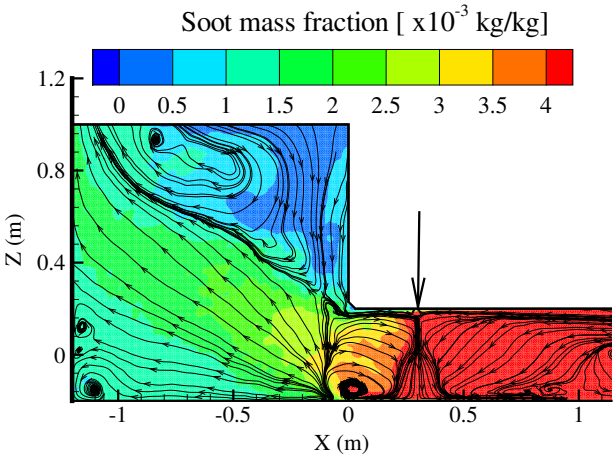

(h) Flow-rate of 122 l/h and $t = 450\ s$

Figure 13: Contour plots of soot mass fraction in the case of HRR of 3.5 kW for different water flow-rates at 380 s and 450 s.

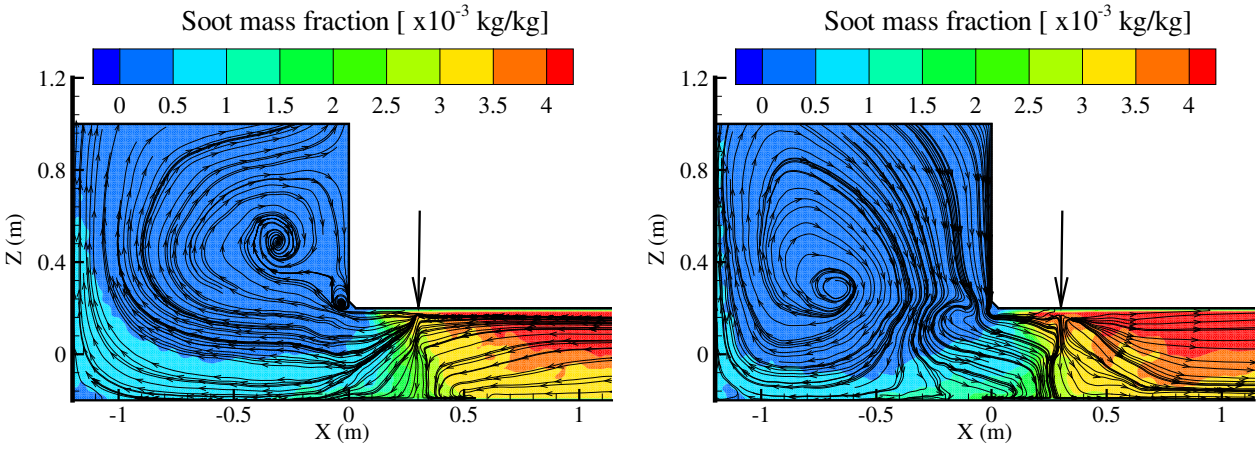

(a) $t = 430\ s$ (b) $t = 450\ s$

Figure 14: Contour plots of soot mass fraction in the case of HRR of 3.5 kW and water flow-rate of 75 L/h.

This behaviour is attributed to the periodic jump of the pressure inside the tunnel. Finally, note that regardless of the considered water flow rate, the spray system fails to block the smoke flow in the small scale configuration.

3.2 Application to the full-scale configuration

As shown in Table 1, the full-scale configuration corresponds to a 500 m long tunnel with a circular cross section of diameter $8.7\ m$. As the selection of the sprinkler system is still an open question for the large scale configuration, a spray with uniform droplet size distribution has been simulated, with droplet diameters set to 1000, 500 and 100 μm successively, in order to investigate the influence of this key parameter. Simulation results are still discussed with the aim to answer to the guiding question: is there any possible smoke confinement in the present conditions.

The spraying water flow rate set by the Société du Grand Paris company is 15 m^3/h. On the basis of the small scale simulation with the corresponding reduced scale flow rate equal to 6 L/h (see Figures 13a ans 13b), one may anticipate that the water mist curtain will not block the smoke flow. In Figure 15, contour plots of temperature are given for the real-scale configuration. This Figure clearly shows that hot smoke flows downstream from the spray zone, toward the wellbore. No significant influence

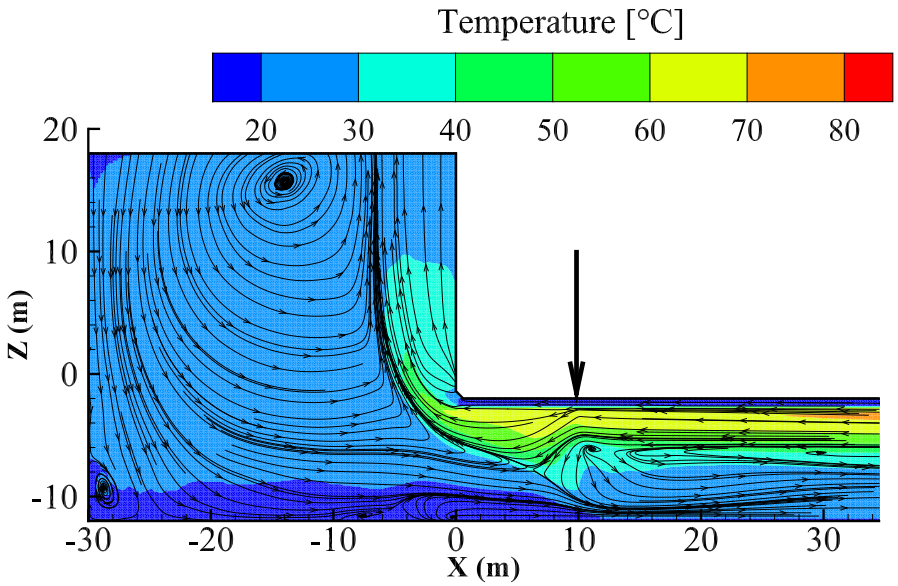

Figure 15: Contour plot of temperature with streamlines in the case of a tunnel of 500 m long and a water flow-rate of 15 m^3/h with uniform distribution of droplets size and a droplet diameter of 500 μm.

of the droplet size was observed. Moreover, a counter current flow is observed in the lower part of the tunnel, similarly to the small scale observations. This counter flow carries soot particles toward the blocked side of the tunnel, which would contribute to penalize the visibility and to increase the toxicity of the environment for any escape or attempt to reach the fire area.

Temperatures were evaluated $5\ m$ downward from the mist system position ($5\ m$ upward from the tunnel exit toward the wellbore), in order to observe the cooling effect of the spraying system. The temperatures are plotted in Figure 16 for different vertical positions and for different droplet diameters. Using these temperature profiles, the smoke layer depth as well as the smoke layer temperature can caluclated using the model by Janssens and Tran (1992). These quantities are plotted in figure (17) for two different position namely at 5m and at 30 m from the exit of the tunnel. It is seen that the cooling of the hot gases is marginal which confirms that the smoke flow is not blocked by the water curtain. The only effect is that the temperature is fluctuating after the spray activation ($t = 300\ s$), probably due due to the mixing induced by the spray. Moreover, it is also observed

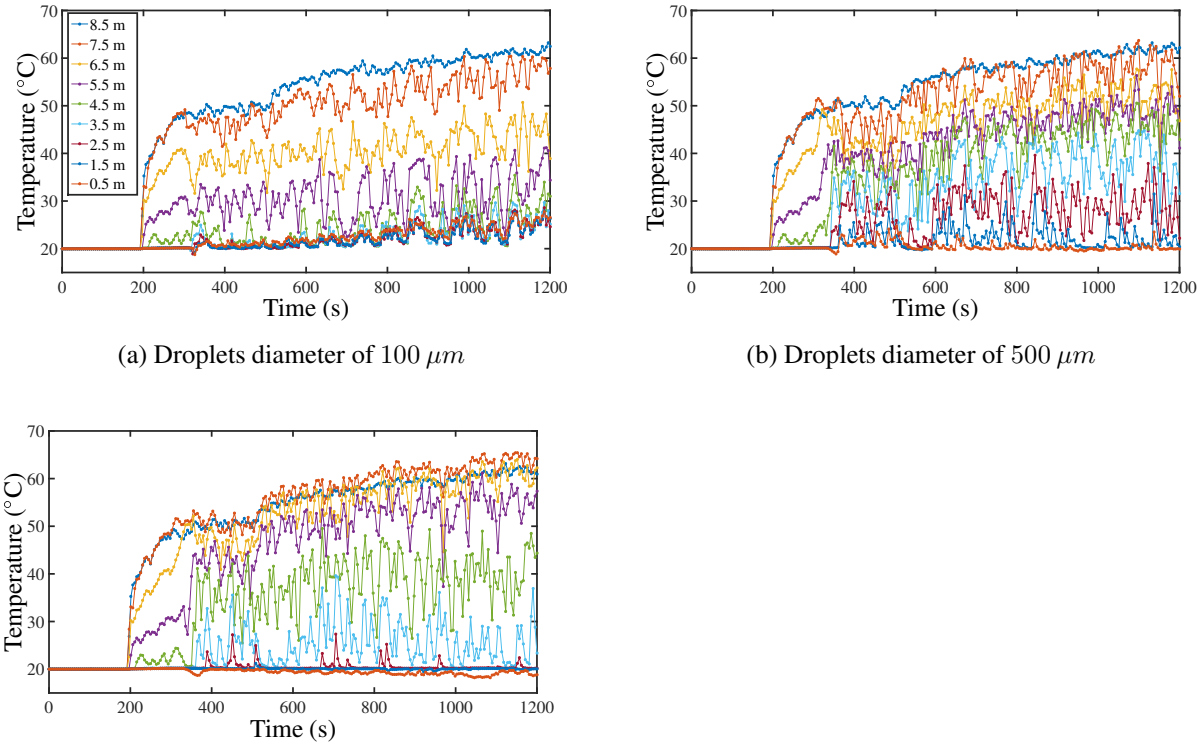

(a) Droplets diameter of 100 μm

(b) Droplets diameter of 500 μm

(c) Droplets diameter of 1000 μm

Figure 16: Time evolution of the temperature at 5 m from the tunnel exit.

that at 30 m from the exit of the tunnel (20 m from the sprinklers), the effect of the droplets size is marginal and all the curves converge to a layer depth of 5 m ($Z_{int} = 3.7\ m$, see figure 17-c). Note that comparisons were conducted with the small scale simulations to confirm this observation, based on simulations in reduced scale with a flowrate of 6.6 L/h and droplet diameter equal to 107 μm, following the scaling rules given in table 1. The obtained temperature variations showed similar fluctuating behavior as in Figure 16b, especially near the interface between the smoke layer and the smoke-free layer.

The total energy absorbed by the water droplets (noted Q_{part}) as well as the energy conducted through walls (noted Q_{cond}) are divided by the fire heat release rate and plotted in figures (18) and (19). As can be observed, the energy absorbed by the spray is always smaller than 5% of HRR. Moreover, this quantity is relatively constant as a function of time and inversely proportional to the droplets diameter.

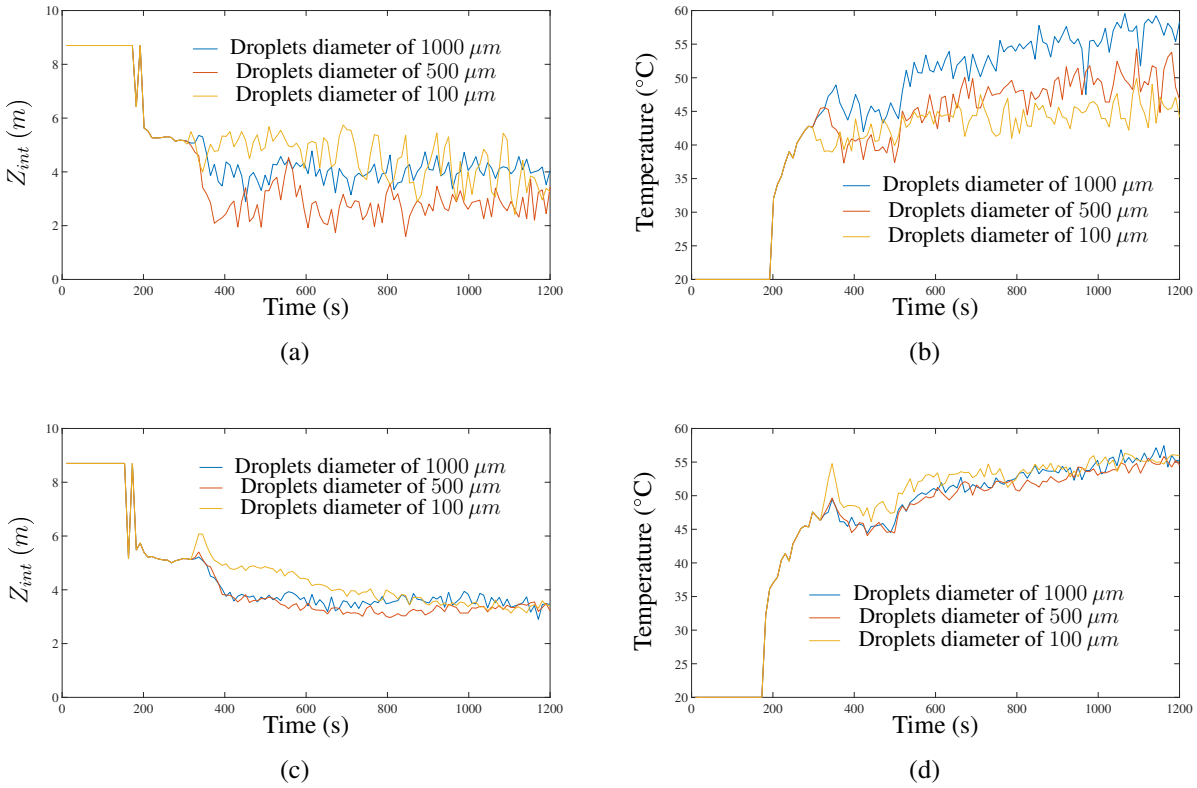

Figure 17: Time evolution of the smoke layer depth for two positions (a) at 5 m and (c) at 30 m from the tunnel exit. Time variation of the smoke layer temperature for two positions (b) at 5 m and (d) at 30 m from the tunnel exit.

Concerning the energy conducted through walls, figure (19) shows that this quantity reaches $30\ \%$ of the fire HRR when the spraying system is absent. When the sprinklers are activated, it is seen that this quantity increases to reach $\simeq\ 35\ \%$ of the fire heat release rate. This fact is due to the confinement effect induced by the spraying system.

4. RADIATION ATTENUATION

Attenuation of radiation from the fire is expected as a second possible advantage of using a water curtain in the tunnel for improving the security level. Absorption and scattering by droplets have

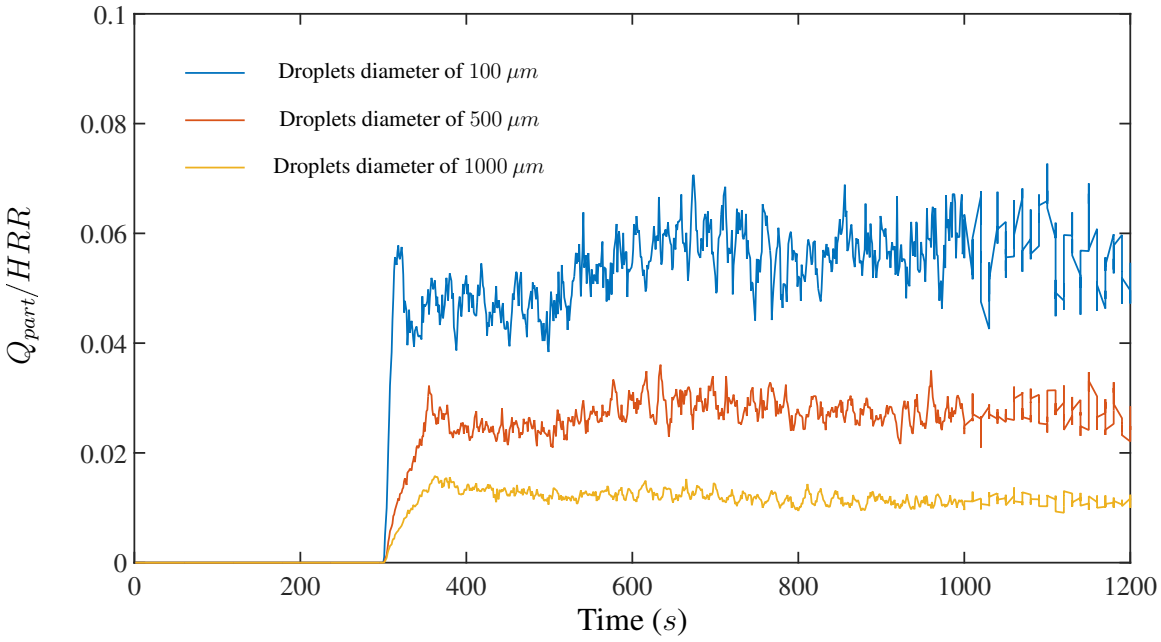

Figure 18: Variation of the ratio between the heat flux absorbed by the droplets Q_{part} and the fire heat release rate HRR, for three different droplets diameter .

been evidenced to result in a significant radiation attenuation (see Dembélé *et al.* (2001); Collin *et al.* (2007, 2010) for example). The resulting attenuation depends on the droplet size distribution, the droplet volume fraction and the water curtain thickness. To provide an evaluation of the variability of the attenuation, simulations were conducted for a wide range of water curtain properties using a Monte Carlo Method for the radiative transfer simulation. The algorithm used in this work is fully detailed in Collin *et al.* (2007).

The curtain is modelled as a collection of droplets with radiative properties defined with the Mie theory (Collin *et al.*, 2005). Only the IR domain is considered, here between 1 and 20 μm, to model radiative transfer. Quanta are then emitted from the radiation source representing the fire area and they are tracked along their path throughout the water curtain, submitted to probabilistic absorption and scattering events until complete absorption or exit of the computational domain. Statistics are performed after tracking of a representative number of quanta to evaluate the remaining energy at

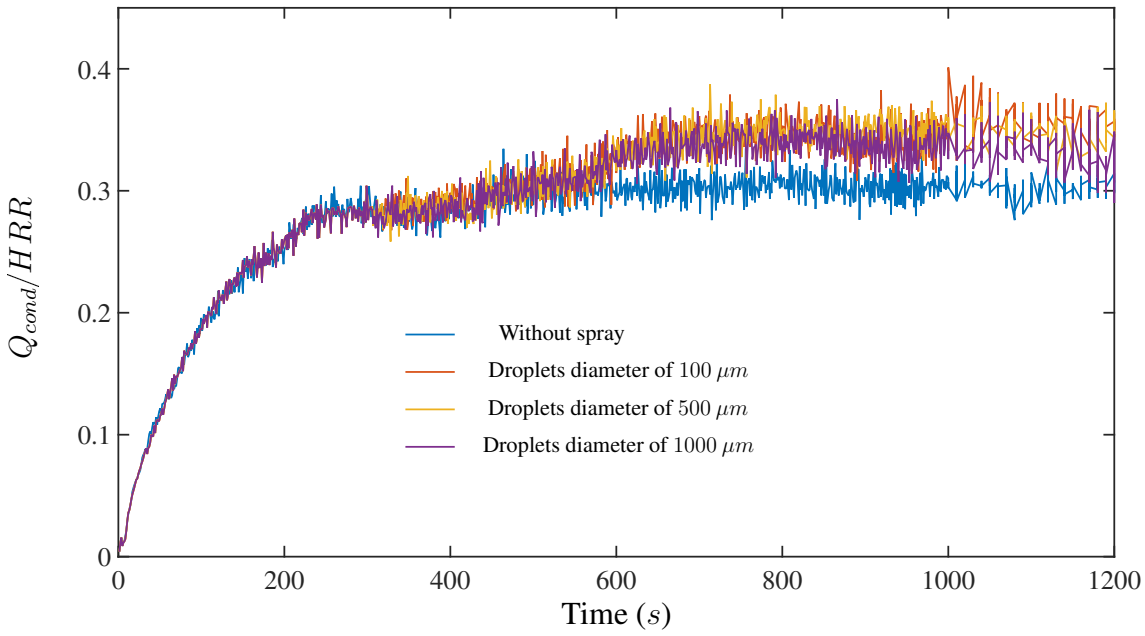

Figure 19: Variation of the ratio between the heat flux conducted through walls Q_{cond} and the fire heat release rate HRR, for three different droplets diameter .

selected positions. The ratio of the energy exiting the curtain divided by the corresponding energy reaching this position without water curtain provides the attenuation ability.

The nominal case was set to a water curtain with a 4 m-thickness, containing a monodisperse distribution of 500 μm droplets with a water volume fraction equal to $5{\cdot}10^{-5}$ m^3/m^3. These features were extracted from the spray patterns provided by FDS, showed in Figure 20. These physical properties are defined to consider a homogeneous waterspray in ensuring that the total water quantity is kept constant. For the present computations the radiation source was set as a black radiant panel with surface equal to the complete cross section of the tunnel (as if the fire was developed across the whole tunnel section in order to be sure that present results would not underestimate the maximum risk with the largest fire source). A characteristic temperature of 1000 K was set for the radiant panel.

Figure 21 gives the spectral attenuation of the nominal spray as a function of wavelength. It can be observed that the spectral attenuation is close to be constant, about 60%, especially for wavelength

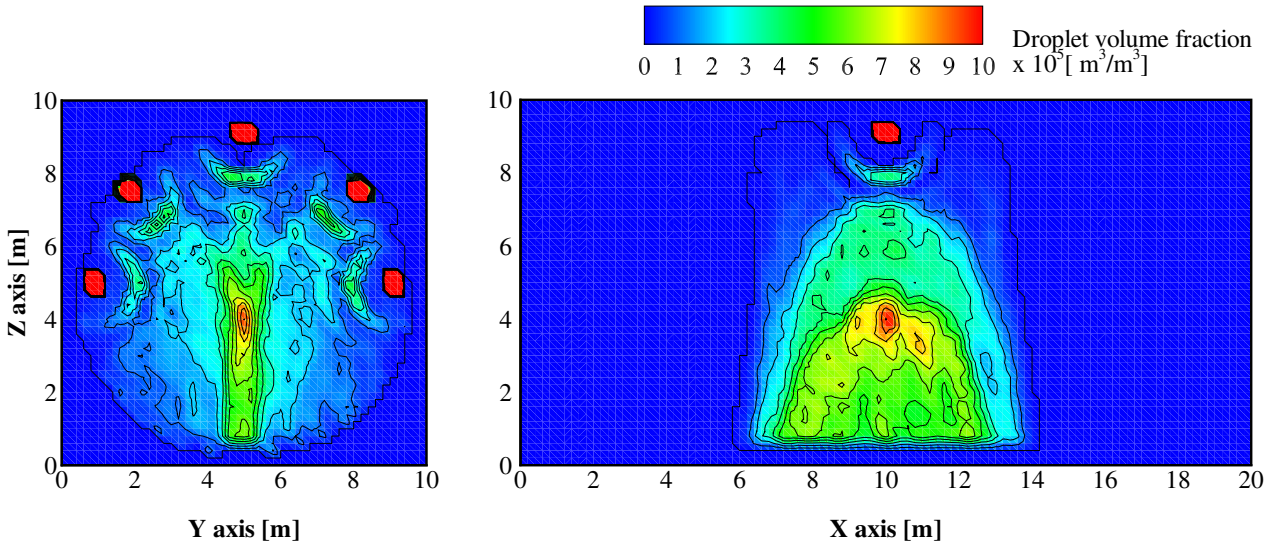

(a) Cross-sectional view

(b) Transverse view

Figure 20: Spray pattern represented by the droplet volume fraction

larger than 3 μm. Absorption and scattering are both involved in the attenuation effect. Their respective contribution depends on the droplet size and concentration. In the present case of quite large droplets, scattering is strongly anisotropic, with a sharp forward-oriented phase function, meaning a weaker efficiency for radiation shielding. This is why absorption contributes to the effective radiation attenuation. Moreover, a detailed analysis done on the reference case demonstrates that the spectral absorbance varies from 27 to 62% on the IR domain whereas the reflectance is in the range between 0 and 6%. In these conditions, radiative absorption by droplets represents between 81 to 100% of radiative extinction performed by a water spray.

The results were used to compute the total attenuation, by integrating the spectral results over the whole spectral range. Planck's averaging was then applied here and the mean radiative attenuation was estimated at 59% for a radiative source set to 1000 K. Additional computations were carried out by varying the temperature between 800 and 1200 K in order to check the influence of this input parameter. Table 4 gathers the average attenuations. A maximum deviation below 4% was found compared to the nominal water curtain for the total attenuation, showing a weak dependence due to

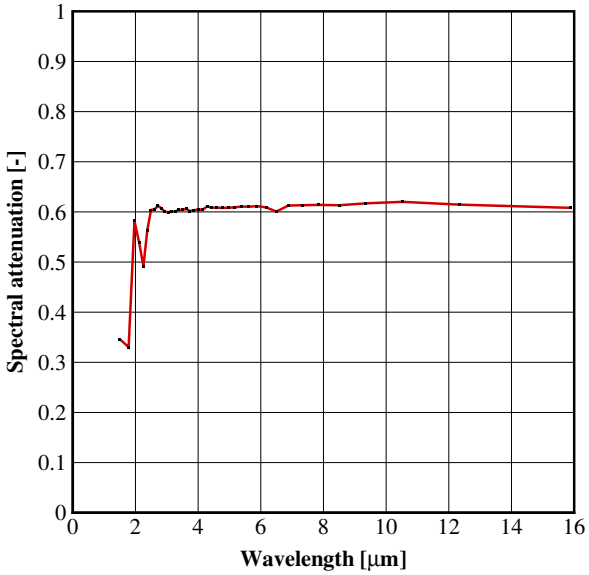

Figure 21: Spectral radiative attenuation of the nominal waterspray (mean diameter: 500 μm, spray width: 4 m, droplet volume fraction: $5{\cdot}10^{-5}$ m^3/m^3)

Source temperature [K]	800	900	1000	1100	1200
Attenuation [%]	60.2	59.5	58.7	57.8	56.7

Table 4: Mean attenuations obtained by Planck's averaging for a range of source temperature from 800 to 1000 K

moderate spectral variations of the droplet radiative properties in the case of interest (as it can be observed in Figure 21).

For a supplementary analysis, the water curtain thickness was varied between 2 and 6 m . These minimum and maximum values were selected, as input parameters aside these ranges would not be achievable in the real scale conditions of interest.

The effect of the spray width is depicted in Figure 22a. The total attenuation rises according to the spray width and varies on a large range from 40% to 70%.

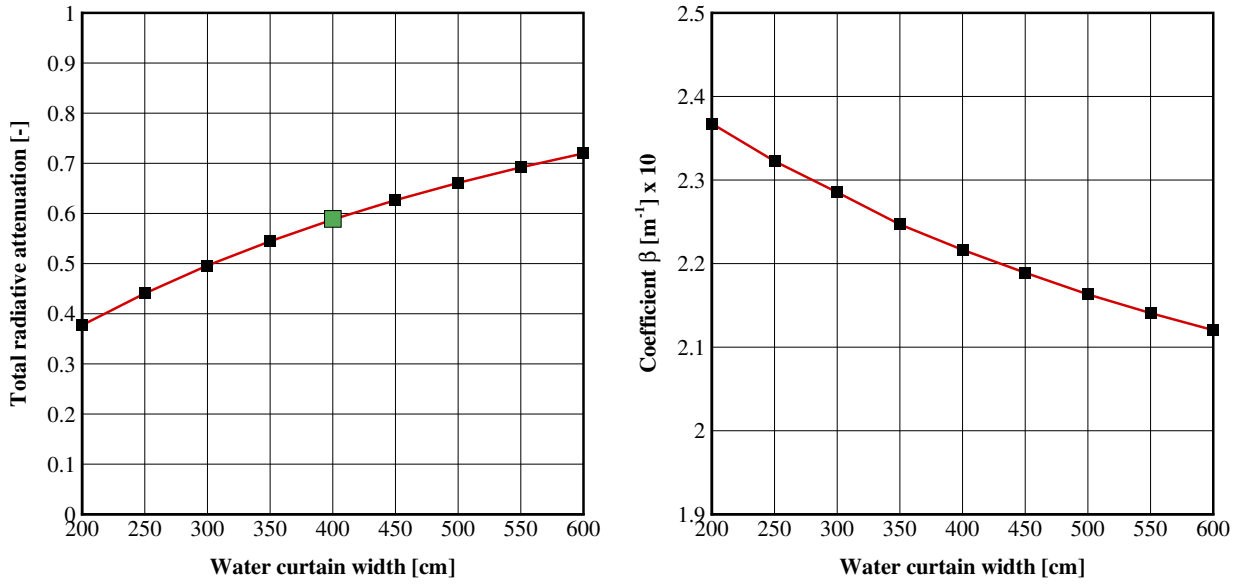

(a) Effect of spray width

(b) estimation of β parameter

Figure 22: Local sensitivity analysis: effect of the spray width on the total attenuation (reference case - mean diameter: 500 μm, spray width: 4 m, droplet volume fraction: $5{\cdot}10^{-5}$ m^3/m^3, source temperature: 1000 K) and effective extinction coefficient β.

It has been previously mentioned that the radiative attenuation provided by these water sprays is mainly due to absorption phenomena. In this configuration, the total attenuation (noted here A) can be estimated knowing the width of the spray (noted here L) and using Beer's law,

$$A = 1 - \exp\left(-\beta L\right) \tag{4}$$

where β is the effective extinction coefficient representing the radiative attenuation of the waterspray. These parameter takes into account the combined effects of the droplet diameter and the droplet volume fraction. Based on the total attenuations presented in Figure 22a, the associated β parameters are plotted in Figure 22b. Obviously, this extinction coefficient weakly varies despite the wide range of water spray widths. A mean value for β can be estimated at 0.221 m^{-1} for a waterspray composed with droplets of 500 μm in diameter and for a volume fraction set to $5{\cdot}10^{-5}$ m^3/m^3.

The spectral extinction coefficient defined by the Mie theory is given by,

$$\beta_\lambda = \pi \frac{d^2}{4} N Q_{\lambda \text{ext}}(d) \tag{5}$$

where, d is the droplet diameter, N the total number of particles in unit volume and $Q_{\lambda \text{ext}}$ the efficiency coefficients for extinction provided by Mie tehory, for instance. As $N = 6\frac{f_v}{\pi d^3}$, the spectral coefficient can be estimated from the droplet volume fraction by,

$$\beta_\lambda = f_v \beta_\lambda^* \tag{6}$$

where β_λ^* depends on the droplet diameter and is expressed as,

$$\beta_\lambda^* = \frac{3}{2d} Q_{\lambda \text{ext}}(d) \tag{7}$$

As it has been previously shown that the spectral attenuation weakly varies on the IR domain, the total attenuation can be estimated by,

$$A = 1 - \exp\left(-\beta^* f_v L\right) \tag{8}$$

For a nominal configuration with a droplet volume fraction set to $5 \cdot 10^{-5}$ m^3 of water / m^3 of air and a spray width to 4 m, different situations were considered in varying the droplet diameter from 100 μm to 1 000 μm. Figure 23 represents, for these different configurations, the evolution of β^* as a function of droplet diameter. β^* decreases when D (droplet diameter) increases. This evolution demonstrates that, for the same amount of water (the same droplet volume fraction), the smallest droplets are more efficient to attenuate the radiative heat flux than the biggest ones. The trend presented by the β^* representation, in Figure 23, seems to follow an exponential law. An attempt was done to fit these data using a least square method, allowing to express β^* coefficient by,

$$\beta^* = \exp\left(-2.1216 \cdot 10^9 D^3 + 5.2691 \cdot 10^6 D^2 - 5.4197 \cdot 10^3 D + 10.0442\right) \tag{9}$$

where D is the droplet diameter expressed in meters. Figure 23 proposes a comparison between the values estimated for β^* and the identified relationship. The calculation of the relative error shows that the maximal discrepancies are lower than 2%, justifying the efficiency of the Eq.(9) to estimate β^*.

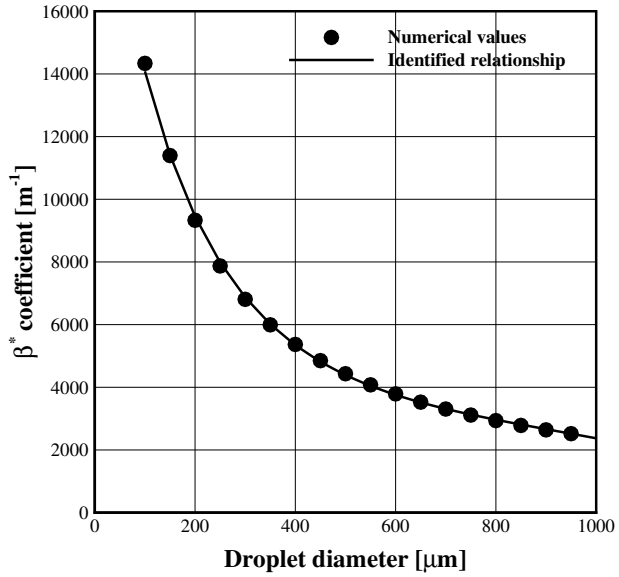

Figure 23: β^* representation function of droplet diameter: comparison between the numerical valued by monte carlo approach and the identified correlation for β^*

In using the relationship defined by Eq.(9) for β^* and the expression of Eq.(8), graphs can be generated representing the radiative attenuation as function a of the spray width and the droplet volume fraction. Two examples, for different droplet diameters, are given in Figure 24. Figures 24a and 24b sum up the results on the attenuation for sprays with droplet diameters set respectively to 100 and 500 μm. Figure 24 shows that the attenuations obtained by sprays with 100 μm-droplets present similar profiles than the ones reached with 500 μm-droplets. For the same spray width, an equivalent radiative attenuation is achieved if the droplet volume fraction of 500 μm-droplets is eight times more important than the one of the spray using 100 μm-droplets.

The previous paragraph demonstrated that the presence of a water spray allows to reduce the radiative heat flux emitted by a fire toward a given target. However, the required safety conditions for evacuees can be also reached if people are moving away from the fire front. As radiation disperses its energy in all the possible propagation directions, the radiative heat flux decreases with the distance from the emitted source. Some additional simulations were done in considering a target, represented by a

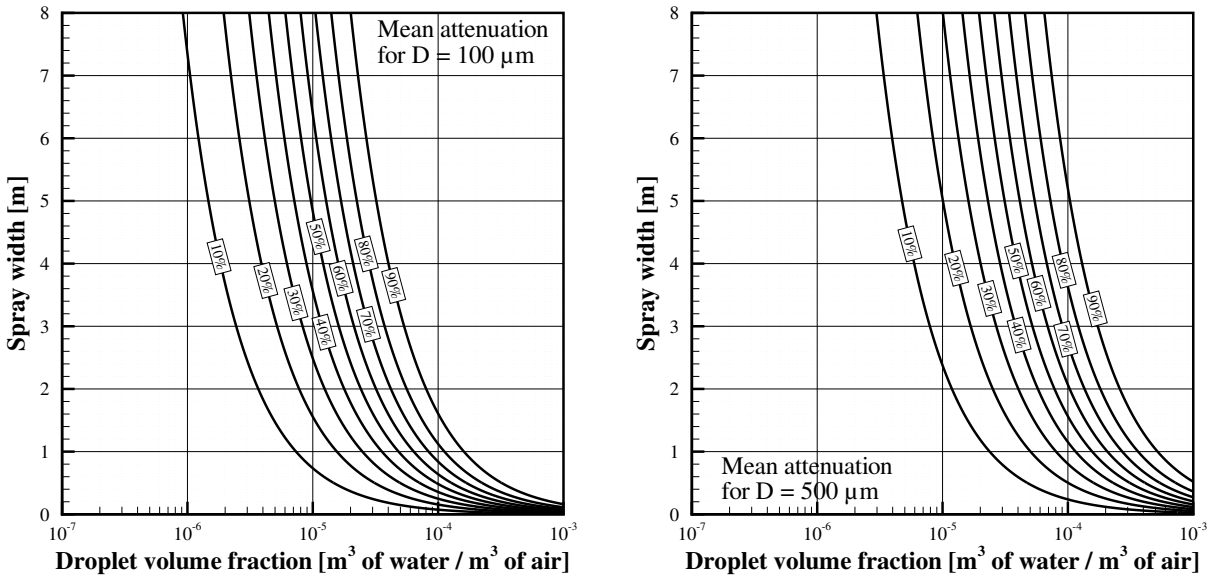

(a) For D = 100 μm

(b) For D = 500 μm

Figure 24: Mean radiative attenuations function of the spray width and the droplet volume fraction, for several droplet diameters

manikin, at different positions from the fire front. The Monte Carlo Approach was used to calculate the radiative heat flux over the manikin area. Figure 25 shows the obtained results for several conditions, 5 m, 10 m and 30 m from the radiative source (without any spray activation). The radiative heat flux emitted by the source is then about 56.7 kW/m^2. Here again, the fire front is assumed to be a blackbody panel at 1000 K. The area of the panel corresponds to the tunnel section. Figure 25 demonstrates that the radiative heat flux is already halved (from 56.7 kW/m^2 to 24 kW/m^2) when the manikin is located at 5 m from fire front. These conditions are not tenable for a person standing and receiving this radiative heat flux without any Personnal Protective Equipment (PPE). It is commonly accepted that beyond 2 - 4 kW/m^2, a person without protection will be in pain. At 30 m, the safety conditions are reached because the maximal radiative heat flux on the manikin is about 1.2 kW/m^2.

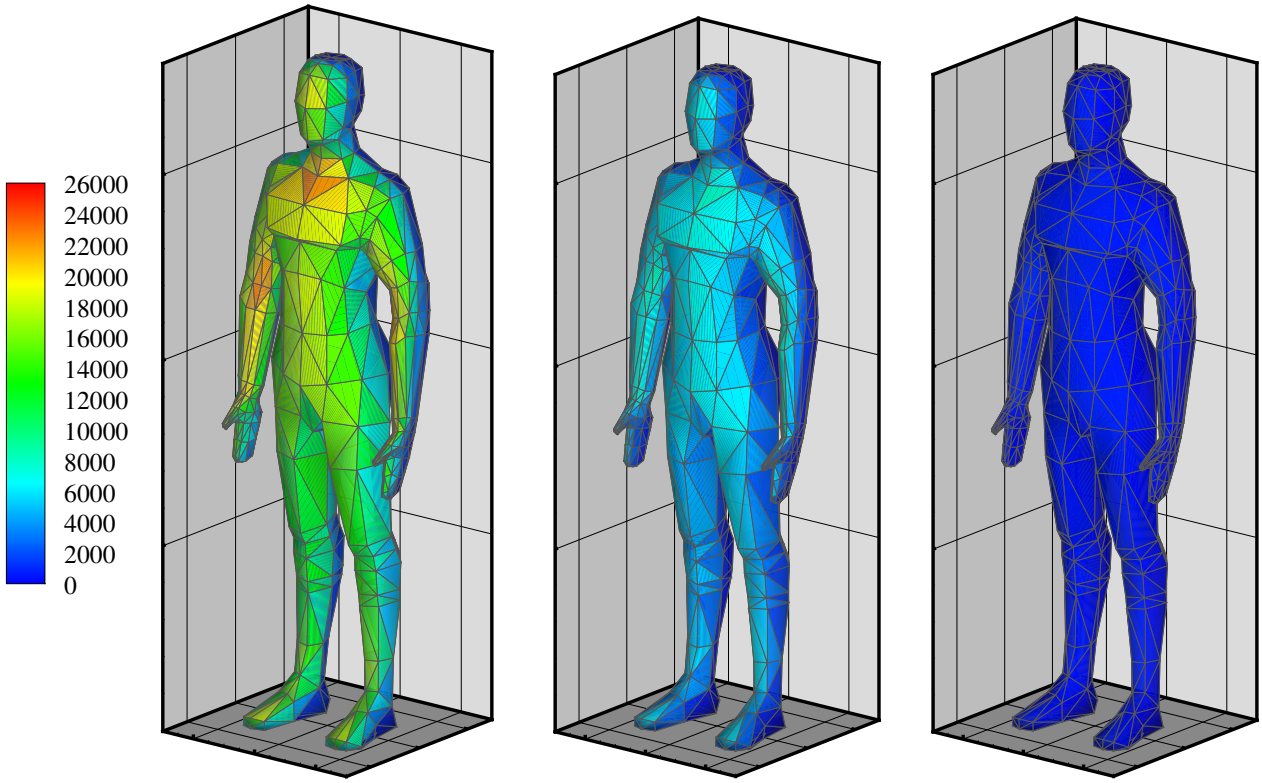

(a) Distance set at 5 m (b) Distance set at 10 m (c) Distance set at 30 m

Figure 25: Radiative heat flux densities (in W/m^2) received by a target located at different positions from the fire front

For each configuration, an attenuation factor can be expressed as,

$$\alpha = 1 - \frac{\varphi_r(x)}{\varphi_r(0)} \tag{10}$$

where, $\varphi_r(x)$ is the maximal radiative heat flux observed over the manikin at a position x from the fire front and $\varphi_r(0)$ is the heat flux emitted by the radiative source. Figure 26 plots the attenuation factor as a function of the distance x. These results show, in a tunnel configuration, that the radiative heat flux quickly decreases. The α coefficient can reaches 80% at 9 m from the fire front and 98% when the target is located at 30 m. Keeping in mind that it would only take around 30 s to escape at such

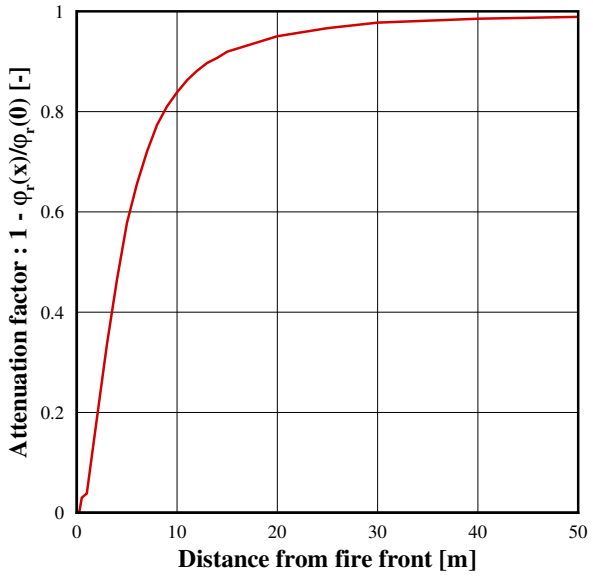

Figure 26: Evolution of the attenuation factor as a function of the distance from the fire front

a distance (for a pedestrian walking at 1 m/s), the water activation would not provide a significant supplementary protection in most cases.

5. CONCLUSIONS

The ability of a water curtain to stop a smoke flow issuing from a fire in a tunnel was studied experimentally and numerically. Experimental investigations were conducted at small scale while numerical simulations were carried out at both small and large scales. Before activating the spray system, a stable stratification of the smoke layer was observed with a smoke layer thickness of 40-50% of the tunnel height at both small and large scale. When the spray was activated, a strong mixing between the ambient fresh air and hot smoke was observed at the spray location. This mixing is due to the drag effect of the spray. Moreover, it was also shown that a flow of fresh air polluted by the smoke flows in the lower part of the tunnel toward the fire.

In all the studied configurations, it was found that the water curtain fails in blocking the smoke flow. It was also found that a criterion based solely on the temperature measurements cannot ascertain the

capacity of a water mist to block the smoke.

It was seen that the water spray can be used to attenuate the radiative heat flux emitted by the fire. With a combination of the appropriate droplet diameter, droplet volume fraction and spray width, large radiative attenuations, up to 90%, can be achieved for realistic configurations.

A simplified model was also derived to estimate the radiative attenuation of a water spray. The model provides mean radiative attenuations with an accuracy higher than 90%.

Finally, this work evaluated that, for the tunnel configurations, the radiative heat flux reduction moving away from the fire, can be very important within the first meters. For instance, a radiative flux reduction by 80% was observed at 9 m from the fire front without use of any supplementary attenuation device.

ACKNOWLEDGEMENTS

The authors would like to thank "Société du Grand Paris" for funding this research and in particular Bertrand Masselin for his support and advice.

APPENDIX

II COMPARISON OF NUMERICAL SIMULATIONS WITH EXPERIMENTS

The objective of this appendix is to compare the experimental results with the numerical data obtained with FDS6. Let us note that only the results for the case of a pool fire of diameter 81 mm will be presented, considering that for the case of a pool fire of diameter of 68 mm, the same observations were made.

Figure 27 shows the temperature measured by the all thermocouple trees in the cases of spraying with a pressure of $4\ bars$ and $1.5\ bars$. In this figure, it is seen that the smoke is cooled stronger with an injection pressure of $4bars$ than an injection pressure of $1.5bars$. Indeed, with such pressure, a greater flow of water is reached and finer droplets are produced. The second effect is related to the smoke mixing, because the drops of water yield a part of their momentum to the surrounding gas. This can be observed on the thermocouple trees 3 and 4 which are arranged upstream and downstream

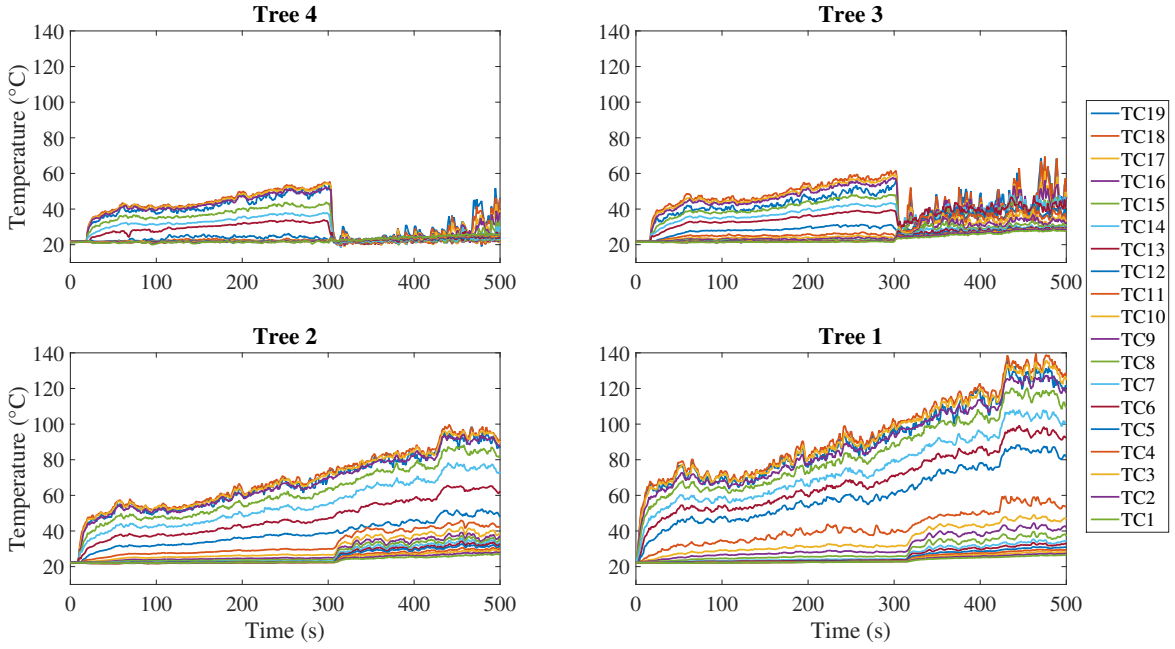

(a)

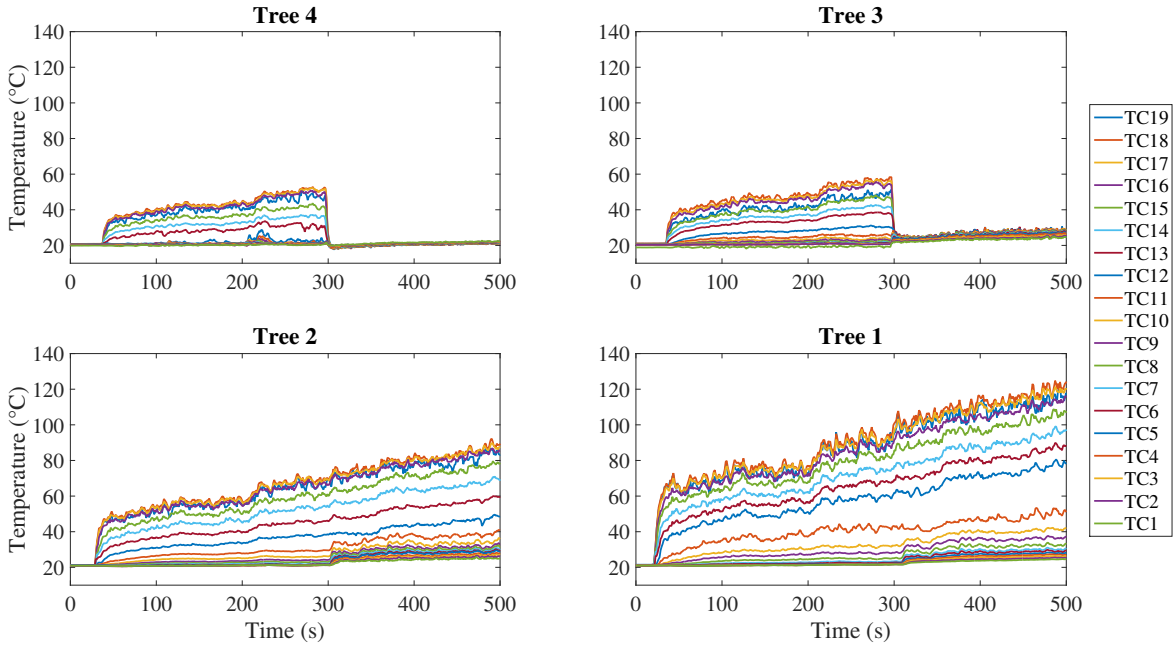

(b)

Figure 27: Time evolution of the temperature for all thermocouple trees in case without spraying and for a pool fire of diameter $81\ mm$ with a pressure nozzle of (a) $1.5\ bars$ and (b) $4\ bars$.

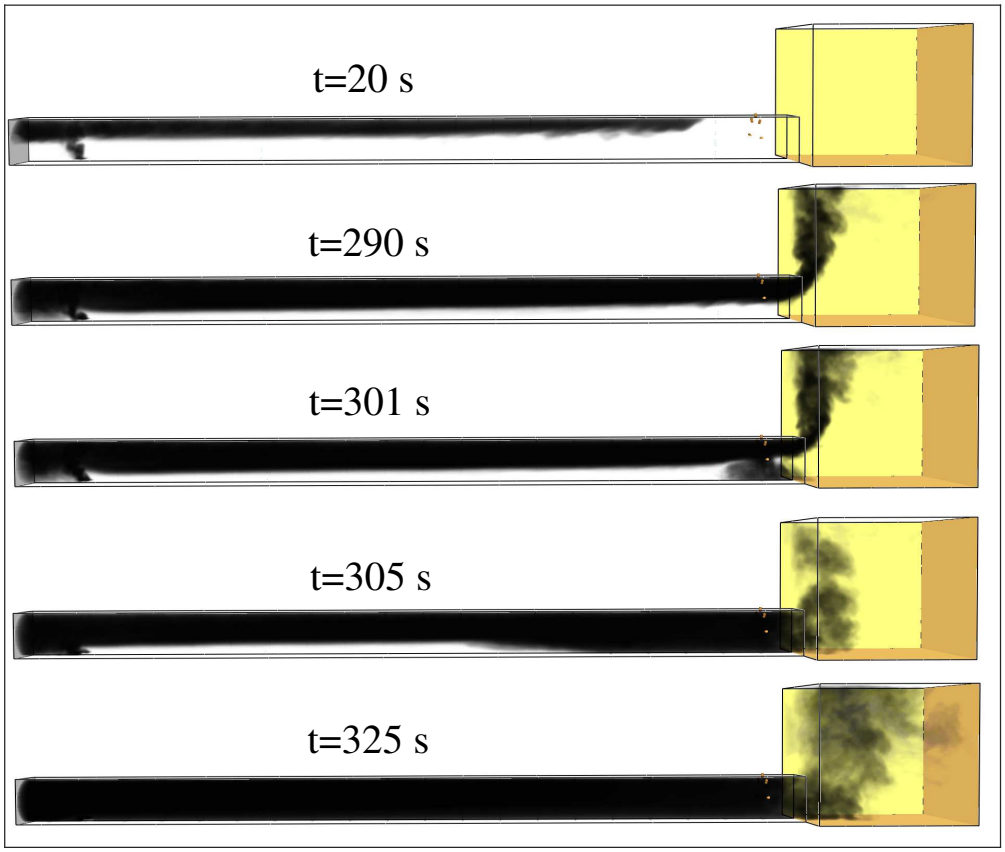

Figure 28: visualisation of the smoke propagation in the case of spraying with a pressure of $4\ bars$, for a pool fire of diameter $81\ mm$

of the spraying system. Indeed, the temperature is homogenized by the strong mixing and cooling induced by the spraying system. This effect is also observed for the case injection pressure of $1.5 bars$. However, it is less intense than the case injection pressure of $4\ bars$. Finally, it can be observed that for trees 1 and 2, no major effect is observed on the temperature measurements in both cases. Indeed, in this zone, the thermal stratification still remains even after the activation of the spraying system.

Concerning the numerical simulations, a visualization of the smoke flow is proposed in figure 28.

This figure present: the early instant of smoke propagation ($20\,s$), before sprinklers activation ($290\,s$), one second after the activation of the sprinklers ($301\,s$) and finally $25\,s$ seconds after the sprinklers activation. The smoke is visualized on the basis of the calculation of the soot concentration provided by SMOKEVIEW. Areas where soot is present in the flow are shown in black color. Qualitatively, smoke production is observed in the zone of fire near the closed end of the tunnel and good reproduction of the stratification of the smoke before sprinkling. After activating the sprinklers, de-stratification in the sprinkling zone is observed, while the smoke continues to flow downstream, demonstrating that the spraying system can not stop the smoke flow. In the end of the simulation, the tunnel appears to be completely filled with smoke. All these observations are consistent with the experimental ones.

More quantitatively, we can analyse the simulation results on the basis of temperature measurements and compare them with the experimental results. Figure 29 show the temperature fields simulated and measured with the same thermocouple trees position as in the experiments in the cases without spraying and spraying with injection pressures of $1.5\,bars$ and $4\,bars$ for the heptane pool of diameter $81\ mm$. Comparison with the experimental results (see figures 27 and 29) shows good overall reproduction by the simulations in terms of temperature growth and of thermal stratification, but with a slightly faster simulated dynamic. The fact that the combustion is probably partly under-ventilated (these mechanisms are difficult to reproduce numerically) or the fire heat release rate is slightly over-estimated in its growth phase may explain the marginal discrepancy between the experiments and the numerical simulations.

Finally in order to perform a more precise comparison between the experimental measurements and numerical simulations, the temperature profiles for all the thermocouple trees have been plot in figures 30, 31, 32 and 33 at different instant in both cases (experimental and numerical) and in the case without spraying. Again, it can be seen that the temperature profiles are broadly similar and in good agreement.

More generally, it can be observed that the calculation on FDS6 satisfactorily reproduces all the physical phenomena induced by the interaction between a spray and a layer of smoke. This

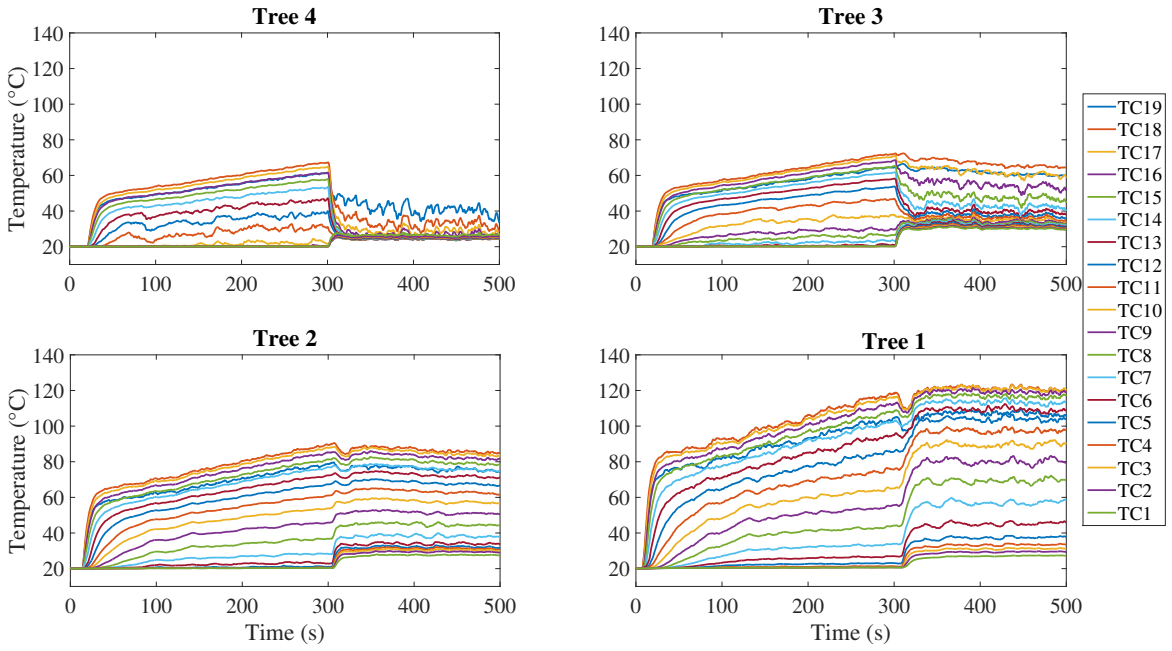

(a)

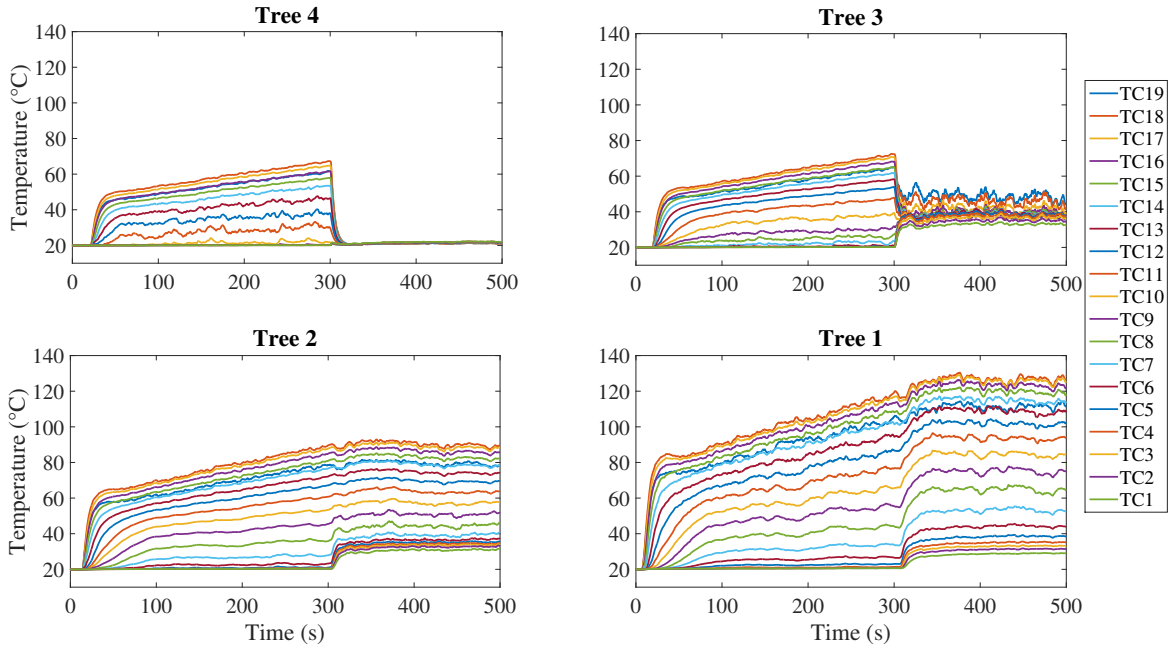

(b)

Figure 29: Time evolution of the temperature for all thermocouple trees in case where spraying system is activated at 300 s for a pool fire of diameter 81 mm with a pressure nozzle of (a) 1.5 $bars$ and (b) 4 $bars$.

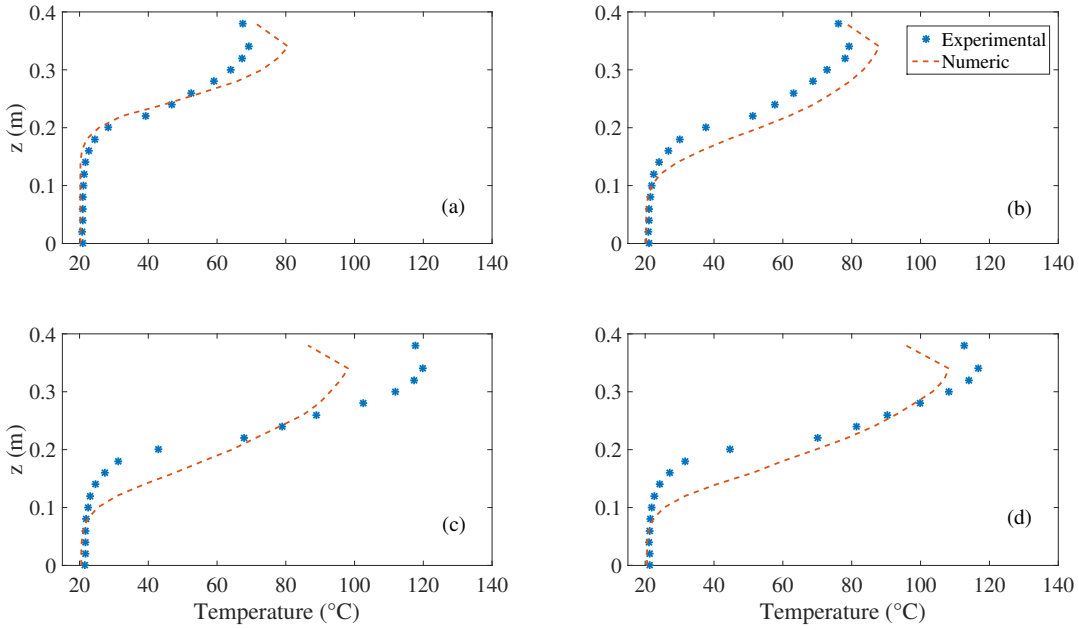

Figure 30: Comparison between numerical simulation and experimental results of temperature profile measured by the tree 1 in a case without spraying for pool fire of diameter $81\ mm$ at different instant: (a) $57s$, (b) $170s$, (c) $340s$ and (d) $500s$.

observation allows us to confidently tackle large-scale simulations.

REFERENCES

Sun, J., Fang, Z., Tang, Z., Beji, T. & Merci, B. (2016) Experimental study of the effectiveness of a water system in blocking fire-induced smoke and heat in reduced-scale tunnel tests. *Tunnelling and Underground Space Technology*, 56, 34-44.

McGrattan, K., Hostikka, S., McDermott, R., Floyd, J., Weinschenk, C. & Overholt, K. (2013) Fire dynamics simulator user's guide *NIST special publication*, 1019, 6th Edition.

Janssens, M.& Tran, H. C. (1992) Data reduction of room tests for zone model validation. *Journal of Fire Sciences*, 10(6), 528-555.

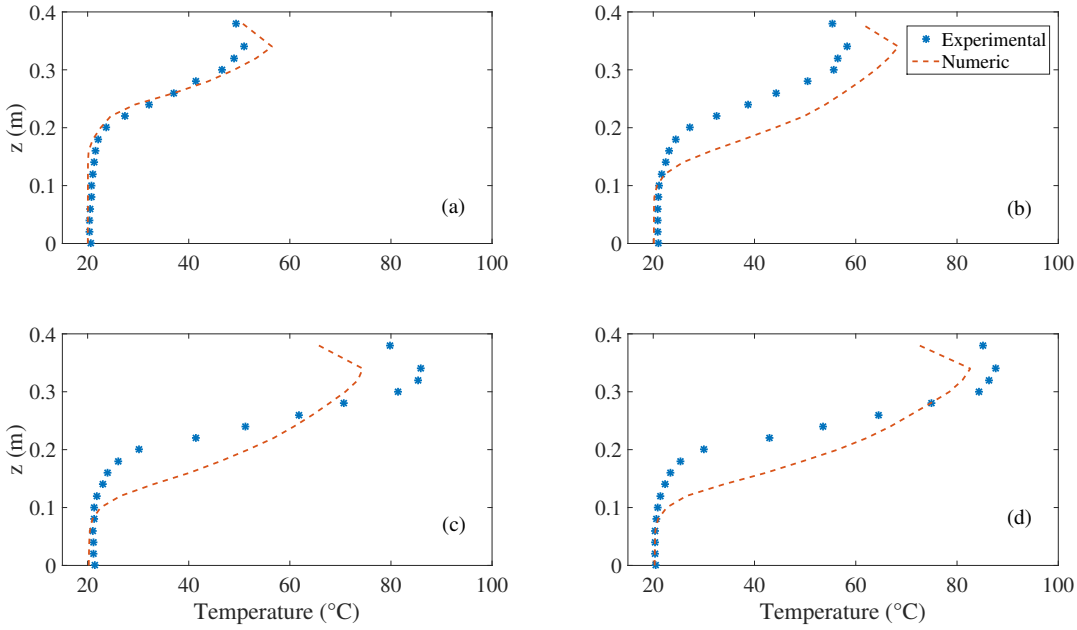

Figure 31: Comparison between numerical simulation and experimental results of temperature profile measured by the tree 2 in a case without spraying for pool fire of diameter $81\ mm$ at different instant: (a) $57s$, (b) $170s$, (c) $340s$ and (d) $500s$.

Lechêne, S., Acem, Z., Parent, G., Jeandel, G. and Boulet, P. (2011) Upward vs downward injection of droplets for the optimization of a radiative shield. *International Journal of Heat and Mass Transfer*, 54(9), 1689-1697.

Blanchard, E., Boulet, P., Fromy, P., Desanghere, S., Carlotti, P., Vantelon, J. P. & Garo, J. P. (2014) Experimental and numerical study of the interaction between water mist and fire in an intermediate test tunnel. *Fire Technology*, 50(3), 565-587.

Ingason, H., Li, Y. Z., Appel, G., Lundström, U. & Becker, C. (2016) Large scale tunnel fire tests with large droplet water-based fixed fire fighting system. *Fire technology*, 52(5), 1539-1558.

Liang, Q., Li, Y., Li, J., Xu, H. & Li, K. (2016) Numerical studies on the smoke control by water mist screens with transverse ventilation in tunnel fires. *Tunnelling and Underground Space Technology*,

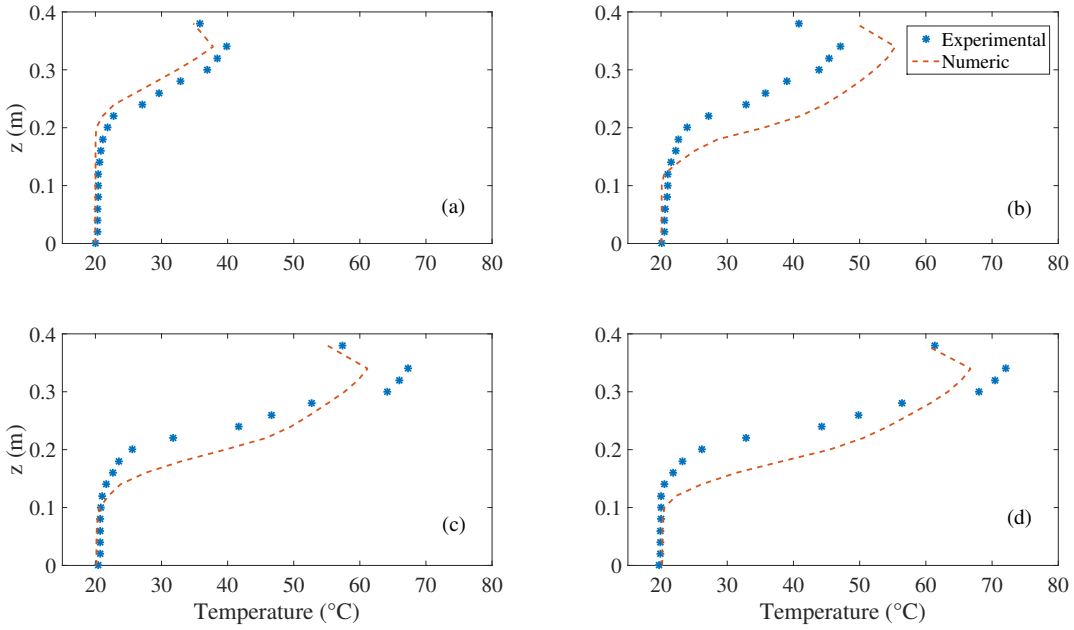

Figure 32: Comparison between numerical simulation and experimental results for temperature profile measured by the tree 3 in a case without spraying for pool fire of diameter $81\ mm$ at different instant: (a) $57s$, (b) $170s$, (c) $340s$ and (d) $500s$.

64, 177-183.

Li, Y. Z. and Ingason, H. (2017) Influence of fire suppression on combustion products in tunnel fires. *Fire Safety Journal*,1-15.

Ingason, H. & Li, Y. Z. (2010) Model scale tunnel fire tests with longitudinal ventilation. *Fire Safety Journal*,45(6), 371-384.

Dembélé, S. Wen, J.X. & Sacadura, J.F. (2001) Experimental study of water sprays for the attenuation of fire thermal. *ASME J. Heat Transfer*, 123, 534-543.

Collin, A., Boulet, P., Lacroix, D. & G. Jeandel (2005) On radiative transfer in water spray curtains using the discrete ordinates method. *Journal of Quantitative Spectroscopy and Radiative Transfer*, 92, 85-110.

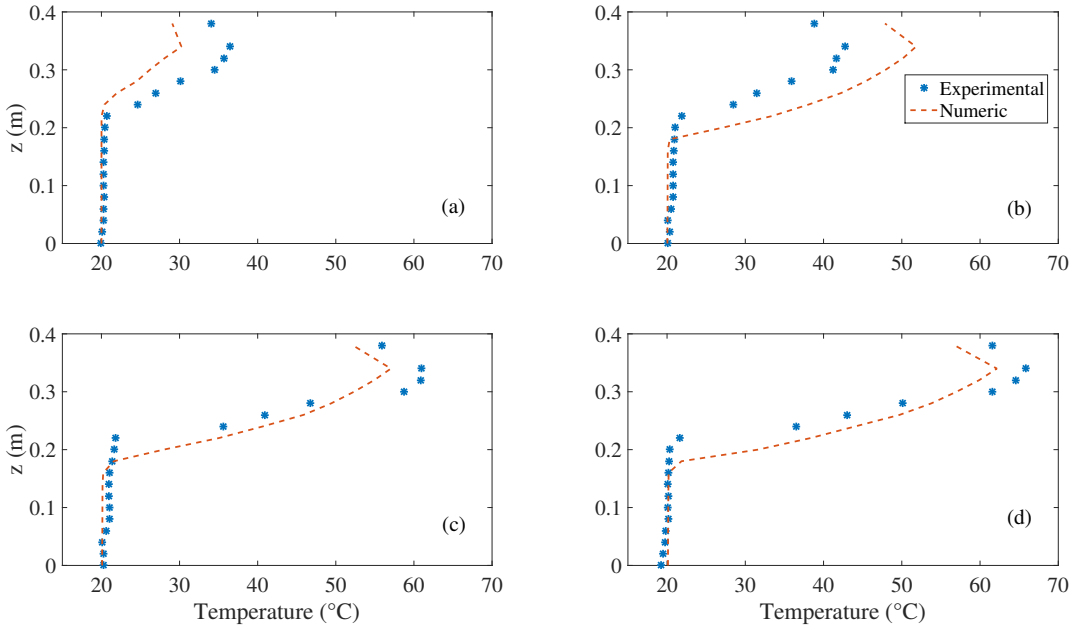

Figure 33: Comparison between numerical simulation and experimental results of temperature profile measured by the tree 4 in a case without spraying for pool fire of diameter $81\ mm$ at different instant: (a) $57s$, (b) $170s$, (c) $340s$ and (d) $500s$.

Collin, A., Boulet, P., Parent, G. & Lacroix, D. (2007) Numerical simulation of a water spray. Radiation attenuation related to spray dynamics. *International Journal of Thermal Sciences*, 46, 856-868.

Collin, A., Lechêne, S., Boulet, P. & Parent, G. (2010) Water mist and radiation interactions : application to a water curtain used as a radiative shield. *Numer. Heat Transfer, Part A.*,57(8), 537-553.

Babrauskas, V. (1983) Estimating large pool fire burning rates. *Fire technology*, 19(4), 251-261.

Wang, Z., Wang, X., Huang, Y., Tao, C., & Zhang, H. (2018) Experimental study on fire smoke control using water mist curtain in channel. *Journal of hazardous materials*, 342, 231-241.

Bullen, M. L. (1977) The effect of a sprinkler on the stability of a smoke layer beneath a ceiling. *Fire technology*, 13(1), 21-34.

Tang, Z., Fang, Z., Yuan, J. P., & Merci, B. (2013) Experimental study of the downward displacement of fire-induced smoke by water sprays. *Fire Safety Journal*, 55, 35-49.

Yang, P., Shi, C., Gong, Z., & Tan, X. (2019) Numerical study on water curtain system for fire evacuation in a long and narrow tunnel under construction. *Tunnelling and underground space technology*, 83, 195-219.

Tang, Z., Fang, Z., & Merci, B. (2014) Development of an analytical model to quantify downward smoke displacement caused by a water spray for zone model simulations. *Fire safety journal*, 63, 89-100.

S. Haouari-Harrak, Mehaddi, R., Boulet, P., Koutaiba, E. M., Giovannelli, G., & Becker, S. (2014) Virtual origin correction for a fire plume in a room under displacement ventilation regime. *International Journal of Thermal Sciences*, 136, 243-253.

He Y., Fernando A. & Luo M. (1998) Determination of interface height from measured parameter profile in enclosure fire experiment *Fire safety journal*, 31(1), 19-38,

Cooper, L. Y., Harkleroad, M., Quintiere, J., & Rinkinen, W. (1982) An Experimental Study of Upper Hot Layer Stratification in Full-Scale Multiroom Fire Scenarios. *Journal of Heat Transfer*, 104(4), 741-749.

Hayasaka H. (1997) Unsteady burning rates of small pool fires. *Proceedings of the 5th Symp. (Int.) on Fire Safety Science*, Melbourne, 1997; 499-510.